View metadata, citation and similar papers at core.ac.uk
brought to you by CORE
provided by NASA Technical Reports Server

(NASA-CR-157053) NUMERICAL SOLUTION OF THE NAVIER-STOKES EQUATIONS FOR BLUNT NOSED BODIES IN SUPERSONIC FLOWS Final Report (Mississippi State Univ., Mississippi State.) 67 p HC A04/MF A01 CSCL 01A G3/02
N78-24045
Unclas
16781

eirs
ENGINEERING & INDUSTRIAL RESEARCH STATION
AEROPHYSICS & AEROSPACE ENGINEERING—MISSISSIPPI STATE UNIVERSITY
Mississippi State, Miss. 39762

# NUMERICAL SOLUTION OF THE NAVIER-STOKES EQUATIONS FOR BLUNT NOSED BODIES IN SUPERSONIC FLOWS

by

Z. U. A. WARSI,
KRISHNA DEVARAYALU AND
J. F. THOMPSON

JUN 1978
RECEIVED
NASA STI FACILITY

Final Report

MSSU-EIRS-ASE-78-1

# COLLEGE OF ENGINEERING ADMINISTRATION

**HARRY C. SIMRALL, M.S.**
DEAN, COLLEGE OF ENGINEERING

**WILLIE L. MCDANIEL, JR., PH.D.**
ASSOCIATE DEAN

**WALTER R. CARNES, PH.D.**
ASSOCIATE DEAN

**LAWRENCE J. HILL, M.S.**
DIRECTOR, ENGINEERING EXTENSION

**CHARLES B. CLIETT, M.S.**
AEROPHYSICS & AEROSPACE ENGINEERING

**WILLIAM R. FOX, PH.D.**
AGRICULTURAL & BIOLOGICAL ENGINEERING

**JOHN L. WEEKS, JR., PH.D.**
CHEMICAL ENGINEERING

**ROBERT M. SCHOLTES, PH.D.**
CIVIL ENGINEERING

**B. J. BALL, PH.D.**
ELECTRICAL ENGINEERING

**W. H. EUBANKS, M.ED.**
ENGINEERING GRAPHICS

**FRANK E. COTTON, JR., PH.D.**
INDUSTRIAL ENGINEERING

**C. T. CARLEY, PH.D.**
MECHANICAL ENGINEERING

**JOHN I. PAULK, PH.D.**
NUCLEAR ENGINEERING

**ELDRED W. HOUGH, PH.D.**
PETROLEUM ENGINEERING

For additional copies or information
address correspondence to

ENGINEERING AND INDUSTRIAL RESEARCH STATION
DRAWER DE
MISSISSIPPI STATE UNIVERSITY
MISSISSIPPI STATE, MISSISSIPPI 39762

TELEPHONE (601) 325-2266

Mississippi State University does not discriminate on the grounds of race, color, religion, sex, or national origin

Under the provisions of Title IX of the Educational Amendments of 1972, Mississippi State University does not discriminate on the basis of sex in its educational programs or activities with respect to admissions or employment Inquiries concerning the application of these provisions may be referred to Dr T K Martin, Vice President, 610 Allen Hall, Drawer J, Mississippi State, Mississippi 39762, or to the Director of the Office for Civil Rights of the Department of Health, Education and Welfare

# Numerical Solution of the Navier-Stokes Equations for Blunt Nosed Bodies in Supersonic Flows

By

Z. U. A. Warsi, Krishna Devarayalu and J. F. Thompson

Report Number MSSU-EIRS-ASE-78-1

Prepared By

Mississippi State University
Engineering and Industrial Research Station
Department of Aerophysics and Aerospace Engineering
Mississippi State, MS 39762

Final Report
Under Contract
NASA Grant NSG 1242
NASA Langley Research Center

May 1978

Table of Contents


| | | Page |
|---|---|---|
| | Abstract | iii |
| | List of Symbols | iv |
| 1. | Introduction | 1 |
| 2. | Numerical Generation of Curvilinear Coordinates | 5 |
| 3. | Formulation of the Problem | 10 |
| 3.1. | Transformation of the Equations | 13 |
| 4. | Finite Difference Approximation and the Solution Algorithm | 16 |
| 4.1. | Numerical Generation of Coordinates | 16 |
| 4.2. | Navier-Stokes Algorithm | 19 |
| 4.2.1. | $\eta$-Derivatives on the Cut | 20 |
| 4.2.2. | Calculation of Wall Density | 22 |
| 4.2.3. | Nonlinear Instability | 23 |
| 4.2.4. | Downstream Boundary Conditions | 23 |
| 4.2.5. | Coordinate Contraction Near a Shock | 24 |
| 5. | Technique of Numerical Solution | 25 |
| 5.1. | Discussion of the Results | 27 |
| 6. | Conclusions | 31 |
| | References | 32 |
| | Appendix-A | 34 |
| | Appendix-B | 38 |
| | Figures | 43 |

Numerical Solution of the Navier-Stokes Equations
for Blunt Nosed Bodies in Supersonic Flows

By

Z. U. A. Warsi, Krishna Devarayalu and J. F. Thompson
Department of Aerophysics and Aerospace Engineering
Mississippi State University
Mississippi State, MS 39762

Abstract

A time dependent, two-dimensional Navier-Stokes code employing the method of body-fitted coordinate technique has been developed for supersonic flows past blunt bodies of arbitrary shapes. The bow shock ahead of the body is obtained as part of the solution, viz., by "shock capturing." A first attempt at mesh refinement in the shock region has been made by using the forcing function in the coordinate generating equations as a linear function of the density gradients. This technique displaces a few lines from the neighboring region into the shock region. Numerical calculations for Mach numbers 2 and 4.6 and Reynolds numbers from 320 to $10^4$ have been performed for a circular cylinder with and without a fairing. In this report results of Mach number 4.6 and Reynolds number $10^4$ for an isothermal wall temperature of 556°K have been presented in detail.

## List of Symbols

| | |
|---|---|
| $A$ | $= \sigma u$, Eq. (3.16) |
| $A_k$ | = Amplitude Factor, Eq. (2.12) |
| $A'_k$ | = Amplitude Factor, Eq. (2.11) |
| $\underset{\sim}{b}$ | = Vector, Eq. (3.4) |
| $B$ | $= \sigma v$, Eq. (3.16) |
| $B_\ell$ | = Amplitude Factor, Eq. (2.12) |
| $B'_\ell$ | = Amplitude Factor, Eq. (2.11) |
| $c_p^*$ | = Specific Heat at Constant Pressure (Dimensional) |
| $C_p$ | = Pressure Coefficient, Eq. (3.29) |
| $\tilde{d}$ | = Deformation Tensor, Eq. (3.4) |
| $D_k$ | = Decay Factor, Eq. (2.12) |
| $D'_k$ | = Decay Factor, Eq. (2.11) |
| $D^{ij}$ | $= \sqrt{g}\, d^{ij}$, $i = 1,2$ , $j = 1,2$ , Eq. (3.10) |
| $e$ | = Non-dimensional Specific Internal Energy |
| $E$ | $= \sqrt{g}\, \Psi$ , Eq. (3.10) |
| $E_\ell$ | = Decay Factor, Eq. (2.12) |
| $E'_\ell$ | = Decay Factor, Eq. (2.11) |
| $f$ | = Scalar Function (Surrogate) |
| $\underset{\sim}{F}$ | = Numerical Vector, Eq. (4.11) |
| $g$ | = Det $(g_{ij})$, Eq. (A-4) |
| $g_{ij}$ | = Covariant Components of the Metric Tensor, Eq. (A-1) |
| $g^{ij}$ | = Contravariant Components of the Metric Tensor, Eq. (A-2) |
| $\underset{\sim}{G}$ | = Numerical Vector, Eq. (4.11) |
| $G_{ij}$ | $= g_{ij}/\sqrt{g}$ |
| $H$ | $= \sigma(u)^2$, Eq. (3.16) |

| | |
|---|---|
| $i, j, \ldots$ | = Used in Index Notation |
| $\tilde{I}$ | = Idem Tensor; Equal to $\delta_{ij}$ when Referred to Cartesian Coordinates and $g_{ij}$ or $g^{ij}$ when Referred to Curvilinear Coordinates, Eq. (3.4) |
| $I$ | = Integers |
| IMAX, JMAX | = Maximum Values of I and J Used |
| $I_{B1}$, $I_{B2}$ | = Values of I where the Cut Meets the Body, Fig. 5 |
| $I_{UC}$, $I_{LC}$ | = Integers Representing I Values on the Upper and Lower Parts of the Cut Respectively, Fig. 5 |
| $J$ | = Integers; also Jacobian where Stated |
| $k^*$ | = Conductivity (Dimensional) |
| $K$ | = $\lambda \operatorname{div} \underset{\sim}{v}$, Eq. (3.4) |
| $m, m'$ | = Number of Points Involved in Attraction Along the $\xi$-Direction, Eqs. (2.11), (2.12) |
| $M$ | = $\sigma(v)^2$, Eq. (3.16) |
| $M_\ell$ | = Local Mach Number, Eq. (3.23) |
| $M_\infty$ | = Freestream Mach Number |
| $\underset{\sim}{n}$ | = Unit Normal Vector, Eq. (B-21) |
| $n, n'$ | = Number of $\eta$-Lines Involved in $\eta$-Line Attraction, Eqs. (2.11), (2.12) |
| $N$ | = $\sigma uv$, Eq. (3.16) |
| $p$ | = Nondimensional Pressure |
| $P$ | = $\sqrt{g}\, p$, Eq. (3.10) |
| $\overline{P}$ | = Function Appearing in Eq. (2.9) |
| $P_r$ | = $\dfrac{\mu^* c^* p}{k^*}$, Prandtl Number, Eq. (3.4) |
| $Q$ | = $(E+P)u$, Eq. (3.16) |
| $\overline{Q}$ | = Function Appearing in Eq. (2.9) |
| $R$ | = $(E+P)v$, Eq. (3.16) |

| | |
|---|---|
| $\underset{\sim}{R}_{I,J}$ | = Numerical Vector, Eq. (4.16) |
| $R_e$ | $= \dfrac{2\rho^*_\infty V^*_\infty R^*_n}{\mu^*_\infty}$, freestream Reynolds Number |
| $R^*_n$ | = Nose Radius (Dimensional) |
| $S_1$ | = Sutherland's Constant, Eq. (3.7) |
| sgn | = Sign Function, Eq. (2.11) |
| $\underset{\sim}{t}$ | = Unit Tangent Vector, Eq. (B-19) |
| $T$ | $= T^*/T^*_\infty$, Nondimensional Temperature |
| $u$ | $= v^1$, Contravariant Velocity Component |
| $v$ | $= v^2$, Contravariant Velocity Component |
| $U,V$ | = Cartesian Velocity Components |
| $v^i$ | = Contravariant Components |
| $v_i$ | = Covariant Components |
| $\underset{\sim}{v}$ | $= \underset{\sim}{v}^*/V^*_\infty$, Nondimensional Velocity Vector |
| $v^i_{,j}$ | = Covariant Derivative |
| $\underset{\sim}{w}$ | = Numerical Vector, Eq. (4.11) |
| $(x,y)$ | = Nondimensional Cartesian Coordinates |
| $x_\ell$ | = Cartesian Coordinates ($x_1 = x$, $x_2 = y$) |
| $\alpha_o$ | = Nondimensional Constant, Eq. (3.4) |
| $\Gamma^i_{jk}$ | = Christoffel Symbols, Eq. (A-7) |
| $\gamma$ | $= c^*_p/c^*_v$, Adiabatic Exponent |
| $\xi,\eta$ | = Transformed Coordinate System |
| $\xi^i$ | = Any Curvilinear Coordinate System, ($\xi^1 = \xi$, $\xi^2 = \eta$) |
| $\xi_k,\eta_k$ | = Values of $\xi$ and $\eta$ for Varying k, Eq. (2.11) |
| $\theta,\phi,\psi$ | = Functions, Eqs. (A-16) - (A-18) |
| $\Psi$ | = Total Energy, Eq. (3.4) |
| $\rho$ | $= \rho^*/\rho^*_\infty$, Nondimensional Density |

| | |
|---|---|
| $\sigma$ | $= \sqrt{g}\,\rho$, Eq. (3.10) |
| $\tilde{\sigma}$ | = Stress Tensor, Eq. (3.4) |
| $\mu$ | $= \mu^*/\mu^*_\infty$, Nondimensional Viscosity |
| $\lambda$ | $= \lambda^*/\mu^*_\infty$, Nondimensional Bulk Viscosity; Also a Surrogate Variable where Stated |
| $\nu^1, \nu^2$ | = Functions, Eq. (3.14), (A-24), (A-25) |
| $\tilde{\tau}$ | = Tensor, Eq. (3.4) |
| $\varepsilon$ | $= 1/R_e$ |
| $\omega$ | = Vorticity; Also as Acceleration Parameter where Stated |
| $\delta_{ij}$ | = Kronecker-$\delta$ |

Operators:

| | |
|---|---|
| div | = Divergence |
| grad | = Gradient |
| $(\ )^T$ | = Transpose |

Subscripts:

| | |
|---|---|
| $\sim$ | = Denotes Vector |
| $\xi, \eta$ | = Partial Differentiation |
| $\infty$ | = Freestream Value |
| w | = Wall Value |
| ij | = Covariant Tensor |
| ,j | = Covariant Derivative |
| i | = Covariant Vector; when used with x or $\xi$, then no Tensorial Significance |
| s | = Stagnation Value |

Superscripts:

| | |
|---|---|
| $\sim$ | = Denotes a Tensor |
| * | = Denotes a Dimensional Quantity |
| ij | = Contravariant Tensor |
| i | = Contravariant Vector |

## 1. Introduction

Numerical solution of the full compressible Navier-Stokes equations for a blunt body placed in a uniform supersonic stream is of much theoretical and practical interest. The problems of viscous compressible flow have been tractable only in the last decade because of the continuing advances in the computer facilities as well as in the numerical methods. A detailed summary of various numerical methods which have been used in the calculation of viscous compressible flow problems has recently been given by Peyret and Viviand [1]. A recent review on blunt body problems by Rusanov [2] is also of interest.

It has been established by experiments that in front of a blunt body placed in a supersonic flow, there appears a detached bow shock wave which separates the flow disturbed by the body from the undisturbed flow. Behind the shock wave there is a subsonic region bounded by it, the body, and the sonic lines emanating near the body. The region behind the sonic lines is again supersonic with the exception of interior shocks and near-body wake. The existence of the subsonic region, with the no-slip condition to be satisfied at the body surface, requires the consideration of full viscous equations. The subsonic region also establishes a direct relationship between the shapes of the nose part of the body and that of shock wave ahead of it.

The present investigation is concerned with the numerical solutions of the complete Navier-Stokes equations for two-dimensional blunt arbitrary shaped bodies placed in moderately high freestream Mach number flows. One of the novel features of the present research is the use of body-fitted numerically generated coordinate systems as developed by Thompson, et. al. [3] and Thames [4]. The coordinate system used in this paper (Ref. to

Figs. 1, 2, and 3) establishes beyond doubt the versatility of the method and the capability of adjustments of the coordinates in regions of interest, such as in the vicinity of a shock or a body surface. Further, the overall problem of analytical development has been rendered more general by using the method of tensor analysis. Thus the extension of the method to three dimensions is now purely formal.

The body-fitted coordinate generation method allows the coordinate lines to be coincident with all the boundaries of a general multiply-connected region including the boundaries formed by solid walls and the external boundaries. Thus with this procedure the numerical solution of the Navier-Stokes equations may be obtained on a fixed rectangular field in the transformed plane without any specification of the mesh sizes, cf. [5]. Further, no interpolation of the flow variables is required regardless of the shape of the physical boundaries or the spacing of the curvilinear coordinate lines in the physical plane.

As noted earlier, the flow in the subsonic region is governed by the shapes of the nose part of the body and that of the shock wave ahead of it. By using the body-fitted coordinate system, the problem of exact specification of the boundary conditions on the nose part of the body is completely resolved. In Sections 2 and 4, both the theory and numerical generation of coordinates are discussed.

The computational domain is now limited upstream by a boundary located at a certain distance ahead of the expected appearance of the bow shock in the steady state. The outer boundary is taken to be a hyperbola placed at a distance about 5.0 of the expected stand-off distance calculated by Van Dyke [6] and Billig [7]. The downstream boundary is a circular arc of radius equal to 5 times the nose radius of the body. An implicit finite-

difference approximation for the non-steady Navier-Stokes equations written in curvilinear coordinates is used to advance the solution from an arbitrary specified solution at time t = 0. Since the position or shape of the shock has not been prescribed a priori, the shock transition region is obtained as part of the solution, i.e., by "shock capturing," as the flow develops. Section 3 describes all the pertinent equations used in the flow calculations while Section 4.2 describes the solution algorithm.

As is usual with any finite-difference solution of the compressible Navier-Stokes equations, the problem of nonlinear oscillations, particularly when a shock exists, is a dominant one. These oscillations or wiggles must be damped by using dissipative finite-difference schemes. McCormack [8], Boris and Book [9], Vliegenthart [10] and others have developed various techniques to damp out the nonlinear oscillations. In the present research we have used both the FCT routine of Ref. [9] and the Shuman filtering of Ref. [10]. It has been found that Shuman filtering works quite well for all the cases considered in this paper, though it has the tendency of lessening the high gradients in the shock region. This aspect of the problem is discussed in Section 4.2.3.

A technique to concentrate the coordinate lines in the vicinity of the shock has been developed. When a quasi steady-state solution has been obtained, the density gradients already known across the shock are then used to re-generate the coordinates and the Navier-Stokes solution is performed on the new coordinates. Though this scheme works quite well, however, because of the limited storage capacity, not many lines could be displaced in the transition region. This aspect is discussed in Section 4.2.5. of this paper.

A series of results on a circular cylinder and a circular cylinder with aft-body have been obtained for several Reynolds and Mach numbers. The wall pressure ratio on a circular cylinder as reported by Tannehill and Holst [11] has been compared with the present solution and the two match fairly well. All numerical results are discussed in Section 5 of this paper. In all cases considered the Knudsen number, $\sqrt{\gamma\pi/2}\, M_\infty/R_e$, is sufficiently small to satisfy the continuum hypothesis.

## 2. Numerical Generation of Curvilinear Coordinates

The accuracy of numerical solutions of the partial differential equations of mathematical physics depends very strongly on our ability to impose the requisite boundary conditions as accurately as possible. For problems of fluid flows past finite bodies, since the boundary values are prescribed on a closed curve forming the body contour (in three dimensions on a closed surface), and also at another closed curve enclosing the given body forming the outer or external boundary, it is natural to envisage a coordinate system in which one coordinate passes exactly through the body contour, and the other passes through the external boundary contour. The idea of numerical coordinate generation is to fill the region with intersecting coordinate lines enclosed by the body and the external boundary contours in the physical (x,y) or (x,y,z) space.

The preceding ideas in one form or another have been used by Winslow [12], Barfield [13], Chu [14], Amsden and Hirt [15], and Godunov and Prokopov [16]. However, the whole concept has been used in a much organized manner to provide a number of solutions in fluid mechanics by Thompson, et. al., [ 3 ], [ 4 ], [ 5 ], [17], [18], [19], [20].

Let $\xi = \xi(x,y)$ and $\eta = \eta(x,y)$ be two continuously differentiable functions of the Cartesian coordinates (x,y). Further, let $\eta = \eta_o$ = constant be the body contour, while $\eta = \eta_\infty$ = constant be the external boundary contour. The region $\eta_o \leq \eta \leq \eta_\infty$ must now be filled by intersecting coordinate curves $\xi$ = constant and $\eta$ = constant. Becuase of the closed region under consideration it is natural to specify the determining differential equations for $\xi$ and $\eta$ as elliptic equations to be solved under the proper boundary conditions for $\xi$ and $\eta$ at the body and at the external boundary. Since the

simplest elliptic equation is the Laplace equation, we then pose the problem of solving the Laplace equations for $\xi$ and $\eta$ with x and y as independent variables under the Dirichlet boundary conditions. Let $\Gamma_1$ be the curve defining the body contour $\eta = \eta_o$ and $\Gamma_2$ be the curve defining the outer boundary $\eta = \eta_\infty$ in the xy-plane as shown in Fig. 1. The elliptic boundary value problem is then

$$\nabla^2 \xi = 0 \tag{2.1}$$

$$\nabla^2 \eta = 0 \tag{2.2}$$

$$\text{on } \Gamma_1: \quad \xi = f_o(x,y), \ \eta = \eta_o \tag{2.3}$$

$$\text{on } \Gamma_2: \quad \xi = f_\infty(x,y), \ \eta = \eta_\infty \tag{2.4}$$

The solutions of Eqs. (2.1) and (2.2) under the boundary conditions (2.3) and (2.4) can conveniently be obtained in those cases when $\eta_o$ and $\eta_\infty$ can be specified by simple analytic methods (such as a circle, ellipse, etc.). To obtain coordinates for arbitrary shaped bodies, it is convenient to transform the Eqs. (2.1) and (2.2) such that x and y are the dependent while $\xi$ and $\eta$ are the independent variables. This transformation can easily be performed for either two or three-dimensional coordinates by the method of tensor analysis and is detailed in Appendix B. Referring to Eqs. (B-13) and (B-14), we find that Eqs. (2.1) and (2.2) are equivalent to

$$g_{22}\, x_{\xi\xi} - 2g_{12}\, x_{\xi\eta} + g_{11}\, x_{\eta\eta} = 0 \tag{2.5}$$

$$g_{22}\, y_{\xi\xi} - 2g_{12}\, y_{\xi\eta} + g_{11}\, y_{\eta\eta} = 0 \tag{2.6}$$

where the variable subscripts denote partial differentiations and the $g_{ij}$ is the metric tensor defined in Appendices A and B. The boundary conditions are now

$$\text{On } \Gamma_1^*: \quad x = F_1(\xi,\eta_o), \ y = F_2(\xi,\eta_o) \tag{2.7}$$

$$\text{On } \Gamma_2^*: \quad x = G_1(\xi,\eta_\infty), \ y = G_2(\xi,\eta_\infty) \tag{2.8}$$

where as shown in Fig. 2, $\Gamma_1^*$ and $\Gamma_2^*$ are the images of the body and the external boundary contours in the $\xi\eta$-plane.

The geometrical meaning of the transformed equations (2.5) and (2.6) is that the body and the external body contours in the xy-plane have been mapped on to the $\xi\eta$-plane which is rectangular. In other words, we can say, that the contours in the xy-plane have been opened up to form the straight lines $\eta = \eta_o$ = constant, and $\eta = \eta_\infty$ = constant in the $\xi\eta$-plane. This can be achieved by imagining a cut connecting the body and the external boundary in the xy-plane as shown in Fig. 1., such that all functions and their derivatives are continuous in crossing the cut. Since a cut line is a part of the field, no boundary conditions can be imposed on $\Gamma_3^*$ and $\Gamma_4^*$ of Fig. 2.

The appearance of $\eta_o$ and $\eta_\infty$ in Eqs. (2.7) and (2.8) is now purely symbolic, denoting the names of the body and of the external boundary respectively. Given the body and the external boundary contours, we can always establish the values of x and y either graphically or analytically for any desired distribution of $\xi$-values. The $\eta$-values can be chosen arbitrarily to form rectangular meshes in the $\xi\eta$-plane.

Equations (2.5) and (2.6) are the basic equations for the generation of coordinates. To have a control over the spacing of the $\xi$ and $\eta$ lines, we envisage another general transformation, say from $\xi,\eta$ to $\xi'$ and $\eta'$. Retaining the $\xi,\eta$ notation, the equations take the form

$$g_{22}\, x_{\xi\xi} - 2g_{12}\, x_{\xi\eta} + g_{11}\, x_{\eta\eta} = \overline{P}x_\xi + \overline{Q}x_\eta \tag{2.9}$$

$$g_{22}\, y_{\xi\xi} - 2g_{12}\, y_{\xi\eta} + g_{11}\, y_{\eta\eta} = \overline{P}y_\xi + \overline{Q}y_\eta \tag{2.10}$$

For details on the above derivations refer to [ 5 ]. The same form of equations are obtained if one starts considering the Poisson equations in place of Eqs. (2.1) and (2.2) and inverts the transformation from x,y to $\xi,\eta$ as independent variables.

The function $\overline{P}$ and $\overline{Q}$ are to some extent arbitrary and can be chosen in various ways to have a desired distribution of coordinates in a given region. In the present research we have made $\overline{P}$ and $\overline{Q}$ to depend on the density gradients to contract the coordinates in the region of the shock. The chosen forms of $\overline{P},\overline{Q}$ are [17]

$$\overline{P} = g \sum_{k=1}^{n'} A_k' \operatorname{sgn}(\xi-\xi_k) \exp(-D_k'|\xi-\xi_k|)$$

$$+ g \sum_{\ell=1}^{m'} B_\ell' \operatorname{sgn}(\xi-\xi_\ell) \exp(-E_\ell' R_\ell) \tag{2.11}$$

$$\overline{Q} = g \sum_{k=1}^{n} A_k \operatorname{sgn}(\eta-\eta_k) \exp(-D_k|\eta-\eta_k|)$$

$$+ g \sum_{\ell=1}^{m} B_\ell \operatorname{sgn}(\eta-\eta_\ell) \exp(-E_\ell R_\ell) \tag{2.12}$$

where

$$g = g_{11}\, g_{22} - (g_{12})^2 = J^2 \tag{2.13}$$

$$R_\ell = [(\xi-\xi_\ell)^2 + (\eta-\eta_\ell)^2]^{1/2} \tag{2.14}$$

The first terms on the right hand sides of both (2.11) and (2.12) are used in the line attraction, while the second terms in both equations are used for the point-attraction. Various terms which appear in these equations have been defined in the "List of Symbols".

In the present research, we have used only the point attraction term of Eq. (2.12) to concentrate the coordinate lines near the shock. The computer program calculates the density difference for all $\eta$-lines in the region of the shock. The amplitude factor $B_\ell$ thus changes according to the position $(\xi,\eta)$ and is defined as

$$B_\ell = (\text{constant})\ (\rho_2-\rho_1)/\rho_1 \tag{2.15}$$

where the subscripts 1 and 2 denote the respective values in the front and behind of that shock which has been computed without coordinate contraction. The constant appearing in (2.15) is selected only once by trial and error and retains the same value for all $\xi$ and $\eta$ positions.

The method of numerical coordinate generation offers much freedom in the orientation of both the $\xi$ and $\eta$ coordinates in the physical xy-plane. For example, the $\eta$ = const. lines can be chosen to go round the body as shown in Fig. 1, or they may not be chosen to form a complete circuit as shown in Fig. 3. However, a choice has to be made in advance of computing the coordinates, because the resulting orientations of the body segment, the cut lines, or the re-entrant segments, and the outer boundary segments in the $\xi\eta$-plane depend on this choice. In the present research we have chosen the coordinate orientation as shown in Fig. 3, in which the front outer boundary is a hyperbolic arc and the rear outer boundary is a circular arc. Figure 4 shows the corresponding segments orientation in the $\xi\eta$-plane. This type of segments orientation requires much care in the computer programing for both the coordinate generation and for the numerical solution of the Navier-Stokes equations. In Section 4 we have discussed the finite-difference approximations of all the equations.

## 3. Formulation of the Problem

For solving the blunt body problem in a general curvilinear coordinate system, we consider the nondimensionalized Navier-Stokes system of equations in the invariant tensor form. The conservation equations are

Mass Conservation:

$$\frac{\partial \rho}{\partial t} + \mathrm{div}(\rho \underset{\sim}{v}) = 0 \tag{3.1}$$

Momentum Conservation:

$$\frac{\partial}{\partial t}(\rho \underset{\sim}{v}) + \mathrm{div}\, \tilde{\tau} = 0 \tag{3.2}$$

Energy Conservation:

$$\frac{\partial \Psi}{\partial t} + \mathrm{div}\, \underset{\sim}{b} = 0 \tag{3.3}$$

where †

$$\tilde{\tau} = \rho \underset{\sim}{v}\underset{\sim}{v} + p\tilde{I} - \varepsilon\tilde{\sigma}$$

$$\underset{\sim}{b} = (\Psi + p)\underset{\sim}{v} - \varepsilon\tilde{\sigma}\cdot\underset{\sim}{v} - \alpha_0 \mu \,\mathrm{grad}\, T$$

$$\Psi = \rho e + \frac{1}{2}\rho|\underset{\sim}{v}|^2$$

$$\tilde{\sigma} = K\tilde{I} + \tilde{d}$$

$$K = \lambda\, \mathrm{div}\, \underset{\sim}{v}$$

† vectors and tensors are denoted by using ~ under and above a symbol respectively.

$$\tilde{d} = \mu \text{def } \underset{\sim}{v} = \mu[\text{grad } \underset{\sim}{v} + (\text{grad } \underset{\sim}{v})^T]$$

$$\varepsilon = 1/R_e$$

$$\alpha_0 = \varepsilon/P_r(\gamma-1)M_\infty^2 \tag{3.4}$$

The nondimensionalized equations (3.1) - (3.4) have been obtained by referring all lengths to the diameter $2R_n^*$; velocity vector, density, viscosity, temperature, enthalpy and pressure to the freestream values $V_\infty^*$, $\rho_\infty^*$, $\mu_\infty^*$, $T_\infty^*$, $h_\infty^*$, and $\rho_\infty^* V_\infty^{*2}$ respectively. Assuming the gas to be calorically and thermally perfect, the equation of state in the non-dimensional variables is

$$p = \frac{\rho T}{\gamma M_\infty^2} \tag{3.5}$$

where $\gamma$ is the adiabatic exponent. Similarly, the nondimensional temperature is given by

$$T = \gamma(\gamma-1)M_\infty^2 \left(\frac{\Psi}{\rho} - \frac{1}{2}|\underset{\sim}{v}|^2\right) \tag{3.6}$$

The relation between temperature and viscosity is provided by the Sutherland formula, which in non-dimensional form is

$$u = \frac{(1+S_1)T^{3/2}}{T + S_1} \tag{3.7}$$

where $S_1 = \frac{S_1^*}{T_\infty^*}$ , $S_1^* = 110°K$ .

Since $\Psi$ is a function of T, hence the system of equations (3.1) - (3.7) form a closed system of equations provided $\lambda = \lambda(\mu)$ is also prescribed. In the present formulation we have used the Stokes' condition

$$3\lambda + 2\mu = 0 \tag{3.8}$$

as the required relation.

The boundary conditions for the system of equations (3.1) - (3.3) are

at the body surface: $|\underset{\sim}{v}| = 0$, $T = T_w$, or $(\frac{\partial T}{\partial n})_w$ specified

$$\Psi_w = \frac{T_w \rho_w}{\gamma(\gamma-1)M_\infty^2}$$

$$p_w = \frac{\rho_w T_w}{\gamma M_\infty^2} \tag{3.9}$$

at freestream infinity: $|\underset{\sim}{v}| = 1$, $\rho = 1$, $T = 1$

$$p = \frac{1}{\gamma M_\infty^2}$$

$$= \frac{1}{2} + \frac{1}{\gamma(\gamma-1)M_\infty^2}$$

In (3.9) the subscript w denotes the wall condition. The density $\rho_w$ is not known in advance but must be obtained by the equations themselves.

Since the governing equations are of parabolic-elliptic type, we therefore need to specify the outflow boundary conditions. In place of specifying the derivative conditions, we have used the complete solution of the Euler equations to specify the downstream boundary condition with

the stipulation that at the outer downstream boundary the effect of viscosity is negligible.

### 3.1 Transformation of the Equations:

The governing equations (3.1) - (3.3) are now transformed to a general coordinate system $\xi^i (i = 1,2)$ by the usual method of tensor analysis.† Using the summation convention on repeated indices, and introducing new dependent variables

$$\sigma = \sqrt{g}\ \rho,\ P = \sqrt{g}\ p,\ D^{ij} = \sqrt{g}\ d^{ij},\ E = \sqrt{g}\ \Psi \tag{3.10}$$

the equations are

$$\frac{\partial \sigma}{\partial t} + \frac{\partial}{\partial \xi^i}(\sigma v^i) = 0 \tag{3.11}$$

$$\begin{aligned}\frac{\partial}{\partial t}(\sigma v^i) + \frac{\partial}{\partial \xi^j}(\sigma v^i v^j) + \Gamma^i_{jk}\sigma v^j v^k &= -\frac{\partial}{\partial \xi^j}(P g^{ij}) \\ &- P\,\Gamma^i_{jk} g^{jk} + \varepsilon\{\frac{\partial}{\partial \xi^j}(K\sqrt{g}\ g^{ij}) \\ &+ \frac{\partial D^{ij}}{\partial \xi^j} + \Gamma^i_{jk}(\sqrt{g}\ K g^{jk} + D^{jk})\}\end{aligned} \tag{3.12}$$

$$\frac{\partial E}{\partial t} + \frac{\partial}{\partial \xi^i}\{(E + P)v^i\} = \varepsilon\frac{\partial}{\partial \xi^i}(\sqrt{g}\ \nu^i) + \alpha_0\frac{\partial}{\partial \xi^i}(\mu\sqrt{g}\ g^{ij}\frac{\partial T}{\partial \xi^j}) \tag{3.13}$$

where $g_{ij}$ is the transformation metric tensor, and

$$\nu^i = K v^i + \mu(g^{ik} g_{jm}\, v^j_{,k} + v^i_{,m})v^m \tag{3.14}$$

†Refer to Appendix A.

In Eqs. (3.10) - (3.14), the superscript indices denote the contravariant components, while a comma denotes the convariant differentiation, i.e.,

$$v^i_{,j} = \frac{\partial v^i}{\partial \xi^j} + \Gamma^i_{jk}\, v^k \tag{3.15}$$

where $\Gamma^i_{jk}$ is the Christoffel symbol.

Equations (3.11) - (3.13) are applicable both to two and three space dimensions. In two dimensions, writing for brevity

$$\begin{aligned} &\xi^1 = \xi,\ \xi^2 = \eta,\ v^1 = u,\ v^2 = v \\ &A = \sigma u,\ B = \sigma v,\ H = \sigma(u)^2,\ M = \sigma(v)^2,\ N = \sigma uv, \\ &Q = (E+P)u,\ R = (E+P)v \end{aligned} \tag{3.16}$$

the equations become of the form

$$\frac{\partial \sigma}{\partial t} + \frac{\partial A}{\partial \xi} + \frac{\partial B}{\partial \eta} = 0 \tag{3.17}$$

$$\frac{\partial A}{\partial t} + \frac{\partial H}{\partial \xi} + \frac{\partial N}{\partial \eta} + \Gamma^1_{11}H + 2\Gamma^1_{12}N + \Gamma^1_{22}M = \theta \tag{3.18}$$

$$\frac{\partial B}{\partial t} + \frac{\partial N}{\partial \xi} + \frac{\partial M}{\partial \eta} + \Gamma^2_{11}H + 2\Gamma^2_{12}N + \Gamma^2_{22}M = \phi \tag{3.19}$$

$$\frac{\partial E}{\partial t} + \frac{\partial Q}{\partial \xi} + \frac{\partial R}{\partial \eta} = \psi \tag{3.20}$$

The expanded form of various terms appearing in Equations (3.17) - (3.20) are given in Appendix A.

The boundary conditions for Equations (3.17) - (3.20) are at the body surface: $u = v = 0$, $T = T_w$, or $(\frac{\partial T}{\partial n})_w$ specified

$$E_w = \frac{T_w\, \sigma_w}{\gamma(\gamma-1)M_\infty^2}$$

$$P_w = (\gamma-1)E_w\ ,$$

at freestream infinity: $u \to y_\eta/\sqrt{g}$ , $v \to -y_\xi/\sqrt{g}$

$$\sigma \to \sqrt{g}$$

$$T \to 1$$

$$P \to \sqrt{g}/\gamma M_\infty^2$$

$$E \to \sqrt{g}\left(\frac{1}{2} + \frac{1}{\gamma(\gamma-1)M_\infty^2}\right) , \tag{3.22}$$

where a $\xi$ or $\eta$ subscript implies partial differentiation.

The local Mach number $M_\ell$ is given by

$$M_\ell = M_\infty |\underset{\sim}{v}|/\sqrt{T} \tag{3.23}$$

where

$$|\underset{\sim}{v}|^2 = g_{11}(u)^2 + 2g_{12}uv + g_{22}(v)^2 \tag{3.24}$$

and

$$T = \gamma(\gamma-1)M_\infty^2 \left(\frac{E}{\sigma} - \frac{1}{2}|\underset{\sim}{v}|^2\right) \tag{3.25}$$

The relations between the local Cartesian and the local contravariant components of the velocity vector $\underset{\sim}{v}$ are

$$U = ux_\xi + vx_\eta$$
$$V = uy_\xi + vy_\eta \ . \tag{3.26}$$

The vorticity $\omega$ is given by the formula

$$\omega = \frac{1}{\sqrt{g}}\left(\frac{\partial v_2}{\partial \xi} - \frac{\partial v_1}{\partial \eta}\right) \tag{3.27}$$

where $v_i$ are the covariant components of $\underset{\sim}{v}$, which are related with the contravariant components as

$$v_i = g_{ij}\, v^j = g_{i1}\, u + g_{i2}\, v \ . \tag{3.28}$$

The pressure coefficient is defined as

$$C_p = \frac{p^* - p_\infty^*}{\frac{1}{2}\rho_\infty^* V_\infty^{*2}} = 2\left(p - \frac{1}{\gamma M_\infty^2}\right) \tag{3.29}$$

## 4. Finite Difference Approximation and the Solution Algorithm

In this section we present the finite difference approximations and the numerical methods used both for the solution of the elliptic system, Eqs. (2.9) - (2.10), and for the complete Navier-Stokes system, Eqs. (3.17) - (3.20).

Before we proceed on the pertinent method of solution, it is important to mention that in the method of body-fitted coordinates it is superfluous to specify the step sizes $\Delta\xi$ and $\Delta\eta$. If IMAX and JMAX represent integers for the maximum numbers of $\xi$ and $\eta$ points respectively in a field, then this input and the desired contraction controlled by the amplitude and decay factors of Eqs. (2.11) - (2.12) decide the variable mesh sizes to be obtained by solving the generating system (2.9) - (2.10). This aspect has been thoroughly discussed in [ 5 ]. Thus the main utility of numerically generated body-fitted coordinates actually lies in the availability of meshes or nets in the $\xi\eta$-plane on which the Navier-Stokes equations are to be solved without specifying the step sizes. Further, the variations both along the $\xi$-and $\eta$-coordinates, are labeled by the consecutive integers in the range $1 \leq I \leq$ IMAX and $1 \leq J \leq$ JMAX.

### 4.1 Numerical Generation of Coordinates:

The solutions of Eqs. (2.9) - (2.10) have been obtained by the Gauss-Siedel method with successive over relaxation (SOR) under the prescribed boundary values for x and y on the body and the external boundary contours, along with the prescribed values of IMAX and JMAX. The spatial derivatives are approximated by the central differences

$$(\lambda_\xi)_{I,J} = (\lambda_{I+1,J} - \lambda_{I-1,J})/2 \tag{4.1}$$

$$(\lambda_{\xi\xi})_{I,J} = (\lambda_{I+1,J} - 2\lambda_{I,J} + \lambda_{I-1,J}) \tag{4.2}$$

where $\lambda$ is a surrogate variable and I,J denote positions along $\xi$ and $\eta$ coordinates respectively. Similar expressions are obtained for $\lambda_\eta$, $\lambda_{\eta\eta}$ and $\lambda_{\xi\eta}$.

The solutions of Eqs. (2.9) - (2.10) yield x and y for the whole flow field as functions of $\xi$ and $\eta$. This data is then used to generate the derivatives $x_\xi$, $x_\eta$, $y_\xi$, $y_\eta$, the metrical coefficients $g_{ij}$, the determinant g, and the Christoffel symbols $\Gamma^i_{jk}$.

It was mentioned in Section 2 that the orientation of the coordinates of the form shown in Fig. 3 requires due care in obtaining derivatives on the cut line. Referring to the schematic shown in Fig. 5 with the x-axis oriented along the cut line, let $I_{UC}$ and $I_{LC}$ denote the integral values of I on the upper and lower parts of the cut respectively. Thus

$$I_{LC} + I_{UC} = IMAX + 1 \ . \tag{4.3}$$

Equation (4.3) establishes the following correspondence between $I_{LC}$ and $I_{UC}$:

| $I_{LC}$ | | $I_{UC}$ |
|---|---|---|
| 1 | Corresponds to | IMAX |
| 2 | " " | IMAX-1 |
| : | | |
| I | " " | IMAX-I+1 |
| : | | |
| $I_{B1}$ | " " | $I_{B2}$ |

(4.4)

where $I_{B1}$ and $I_{B2}$ represent the same point of the body reached by the lower and upper parts of the cut respectively. Obviously

$$I_{B2} = (IMAX + 1) - I_{B1} \ .$$

From (4.4), we conclude that

$$x(I_{UC},J) = x(I_{LC},J) \tag{4.5}$$

and

$$x(I_{UC}+1,J) = x(I_{LC}-1,J) \tag{4.6}$$

The first derivatives on the lower and upper parts of the cut are

$$(x_\xi)_{LC} = \frac{1}{2}\,[x(I_{LC}+1,1) - x(I_{LC}-1,1)]$$

$$(x_\eta)_{LC} = \frac{1}{2}\,[x(I_{LC},2) - x(I_{UC},2)]$$

$$(y_\xi)_{LC} = \frac{1}{2}\,[y(I_{LC}+1,1) - y(I_{LC}-1,1)]$$

$$(y_\eta)_{LC} = \frac{1}{2}\,[y(I_{LC},2) - y(I_{UC},2)] \tag{4.7}$$

where $2 \le I_{LC} \le I_{B1} - 1$ .

$$(x_\xi)_{UC} = \frac{1}{2}\,[x(I_{UC}+1,1) - x(I_{UC}-1,1)]$$

$$(x_\eta)_{UC} = \frac{1}{2}\,[x(I_{UC},2) - x(I_{LC},2)]$$

$$(y_\xi)_{UC} = \frac{1}{2}\,[y(I_{UC}+1,1) - y(I_{UC}-1,1)]$$

$$(y_\eta)_{UC} = \frac{1}{2}\,[y(I_{UC},2) - y(I_{LC},2)] \tag{4.8}$$

where

$$I_{B2} + 1 \le I_{UC} \le IMAX - 1 .$$

Using (4.6) in (4.8), we find that

$$(x_\xi)_{UC} = -\,(x_\xi)_{LC}$$

$$(y_\xi)_{UC} = -\,(y_\xi)_{LC} = 0$$

$$(x_\eta)_{UC} = -\,(x_\eta)_{LC} = 0$$

$$(y_\eta)_{UC} = -\,(y_\eta)_{LC} \tag{4.9}$$

From the definition of $\Gamma^i_{jk}$ given in Eq. (B-6) we find that on the cut line

$$\Gamma^1_{12} = \Gamma^2_{11} = \Gamma^2_{22} = 0 \tag{4.10}$$

4.2 Navier-Stokes Algorithm:

The Navier-Stokes equations (3.17) - (3.20) can be put in the numerical vector form as

$$\frac{\partial \underset{\sim}{w}}{\partial t} + \frac{\partial \underset{\sim}{F}}{\partial \xi} + \frac{\partial \underset{\sim}{G}}{\partial \eta} + \underset{\sim}{H} = 0 \tag{4.11}$$

where

$$\underset{\sim}{w} = \begin{Bmatrix} \sigma \\ A \\ B \\ E \end{Bmatrix} \tag{4.12}$$

$$\underset{\sim}{F} = \begin{Bmatrix} A \\ H \\ N \\ Q \end{Bmatrix} \tag{4.13}$$

$$\underset{\sim}{G} = \begin{Bmatrix} B \\ N \\ M \\ R \end{Bmatrix} \tag{4.14}$$

$$\underset{\sim}{H} = \begin{Bmatrix} \Gamma^1_{11} H + 2\Gamma^1_{12} N + \Gamma^1_{22} M - \theta \\ \Gamma^2_{11} H + 2\Gamma^2_{12} N + \Gamma^2_{22} M - \phi \\ - \psi \end{Bmatrix} \tag{4.15}$$

We now discretize Eq. (4.11) by a fully implicit difference approximation. The time derivative is approximated by a first-order backward difference at n+1, where n is the time step of size $\Delta t$, while the spatial derivatives are approximated by central differences. The system of equations are solved by point-SOR, which are

$$\underset{\sim}{w}_{I,J}^{n+1} = \underset{\sim}{w}_{I,J}^{n+1(p)} + \omega \underset{\sim}{R}_{I,J} \tag{4.16}$$

where $\omega$ is the relaxation parameter and the superscript (p) denotes values at the previous iteration. The function $\underset{\sim}{R}$ is

$$\underset{\sim}{R}_{I,J} = \underset{\sim}{w}_{I,J}^{n} - \underset{\sim}{w}_{I,J}^{n+1(p)} - \frac{\Delta t}{2} \{\underset{\sim}{F}_{I+1,J}^{n+1} - \underset{\sim}{F}_{I-1,J}^{n+1}$$

$$+ \underset{\sim}{G}_{I,J+1}^{n+1} - \underset{\sim}{G}_{I,J-1}^{n+1}\} - (\Delta t)\, \underset{\sim}{H}_{I,J}^{n+1} \tag{4.17}$$

where the values of $\underset{\sim}{w}$ in $\underset{\sim}{F}$, $\underset{\sim}{G}$ and $\underset{\sim}{H}$ are those which are the most recent values available from the previous iteration. Fully expanded forms of (4.17) are given in [21].

### 4.2.1 <u>$\eta$-Derivatives on the Cut</u>:

To find the $\eta$-derivatives on the cut, we refer to Fig. 6. The point 1 of the physical plane goes on to the point x of the transformed plane, while point 2 remains at its position. Thus in principle, the function value at the fictitious point shown under the lower cut must be replaced by the function value at the point 2 on the upper cut. Now two cases arise depending on whether the function is a scalar (like pressure, temperature, etc.,) or a vector.

For a scalar f, the first $\eta$-derivatives are

$$\left(\frac{\partial f}{\partial \eta}\right)_{I_{LC},1} = \frac{1}{2}\,[f(I_{LC},2) - f(I_{UC},2)]$$

$$\left(\frac{\partial f}{\partial \eta}\right)_{I_{UC},1} = \frac{1}{2}\,[f(I_{UC},2) - f(I_{LC},2)]$$

Thus

$$\left(\frac{\partial f}{\partial \eta}\right)_{I_{LC},1} = -\left(\frac{\partial f}{\partial \eta}\right)_{I_{UC},1} \tag{4.18}$$

Similarly, the second $\eta$-derivatives are

$$\left(\frac{\partial^2 f}{\partial \eta^2}\right)_{I_{LC},1} = f(I_{LC},2) - 2f(I_{LC},1) + f(I_{UC},2) \tag{4.19}$$

$$\left(\frac{\partial^2 f}{\partial \eta^2}\right)_{I_{UC},1} = f(I_{UC},2) - 2f(I_{UC},1) + f(I_{LC},2) \tag{4.20}$$

But f is a scalar, so that

$$f(I_{LC},1) = f(I_{UC},1)$$

hence both (4.19) and (4.20) represent the same value.

To find the $\eta$-derivatives of a directional quantity u on the cut, we need the value of u at the fictitious point. Since in the physical plane u in the lower part of the cut is directed opposite to that on the upper part of the cut, hence

$$\left(\frac{\partial u}{\partial \eta}\right)_{I_{LC},1} = \frac{1}{2}\,[u(I_{LC},2) - (-u(I_{UC},2))]$$

$$= \left(\frac{\partial u}{\partial \eta}\right)_{I_{UC},1} \tag{4.21}$$

The same holds for v, $x_\xi$, $x_\eta$, $y_\xi$ and $y_\eta$.

Based on the preceding analysis it is easy to show that either for a scalar function f or a vector function $\underset{\sim}{v}$ the derivatives across the cut are continuous.

4.2.2 Calculation of Wall Density:

The wall density is calculated by evaluating each term of the continuity equation (3.17) at the body surface. Denoting by J=1 the body surface, we have

$$\left(\frac{\partial\sigma}{\partial t}\right)^{n+1}_{I,1} = -\left(\frac{\partial B}{\partial \eta}\right)^{n+1}_{I,1}$$

Using a three-point forward difference approximation for the right hand side, we obtain

$$\sigma^{n+1}_{I,1} = \sigma^{n}_{I,1} - \frac{\Delta t}{2}\left(4B^{n+1}_{I,2} - B^{n+1}_{I,3}\right) \tag{4.22}$$

where $B^{n+1}_{I,1} = 0$ .

Though Eq. (4.22) is fully implicit, nevertheless its use at the trailing edge point always produces unrealistic density values. To circumvent this difficulty, we used Eq. (4.22) at all points of the body except at the trailing edge point where we have used an explicit scheme based on the leap-frog method

$$\left(\frac{\partial\sigma}{\partial t}\right)^{n}_{I,1} = -\left(\frac{\partial B}{\partial \eta}\right)^{n}_{I,1}$$

$$\frac{\sigma^{n+1}_{I,1} - \sigma^{n-1}_{I,1}}{2\Delta t} = -\frac{1}{2}\left(B^{n}_{I,2} - B^{n}_{I,0}\right)$$

where '0' is a fictitious point. Using a second order extrapolation in space and time, we get

$$B^{n}_{I,0} = 2B^{n-1}_{I,1} - B^{n-2}_{I,2}$$

Thus the wall density is obtained by the expression

$$\sigma^{n+1}_{I,1} = \sigma^{n}_{I,1} - \Delta t\left(B^{n}_{I,2} + B^{n-2}_{I,2}\right) \tag{4.23}$$

### 4.2.3 Nonlinear Instability

In the calculation of compressible flows, several types of nonlinear instabilities are encountered. Among these, the most dominant is due to the difference approximation to the convective derivative. It is a matter of experience that the convective instability can be avoided by introducing some dissipation in the difference approximation of the differential equation being solved. In this context, McCormack [8] has used a fourth-order damping term for his explicit schemes. Boris and Brook [9] have developed a flux-corrected transport (FCT) technique which is quite efficient for use in the continuity equation. Vliegenthart [10] and Harten and Zwas [22] have used the "Shuman filtering" to supress the convective instabilities.

In the present research we have tried both the FCT of Ref. [9] and the Shuman filtering of Ref. [10]. Though the Shuman filter adds more dissipation than desired, particularly near the shock, it always produced wiggles-free solutions for all regions of the flow field. The application of Shuman filter amounts to replacing the vector $\bar{\underset{\sim}{w}}^n_{I,J}$, defined by $\underset{\sim}{w}^n_{I,J} = \sqrt{g}\,\bar{\underset{\sim}{w}}^n_{I,J}$, in (4.17) by

$$\frac{1}{8}\left[\bar{\underset{\sim}{w}}^n_{I+1,J} + \bar{\underset{\sim}{w}}^n_{I-1,J} + \bar{\underset{\sim}{w}}^n_{I,J+1} + \bar{\underset{\sim}{w}}^n_{I,J-1} + 4\,\bar{\underset{\sim}{w}}^n_{I,J}\right] \qquad (4.24)$$

### 4.2.4 Downstream Boundary Conditions:

For the solution of the parabolic-elliptic system of equations (3.17) - (3.20), beside the boundary conditions at the body surface and at the upstream free boundary (Eqs. (3.22)), it is also necessary to specify a proper set of conditions at the downstream boundary. To obtain these conditions, we have placed the downstream boundary at a sufficient distance where the viscous dissipation is negligibly small and have solved the complete Euler's equations for the whole boundary. The computer program has been structured in such a way that is solves both the Navier-Stokes and Euler's equations simultaneously.

4.2.5 Coordinate Contraction Near a Shock:

The capability of attracting the coordinate lines to other pre-designated coordinate lines or grid points exists at present and through the application of this technique to blunt body flows with strong shocks an effort was made to concentrate in, and define, the region of the shock. The magnitude of concentration is controlled by the factors $B_\ell$ and $E_\ell$ defined in Eq. (2.12). These coordinate control factors were expressed as functions of the local density gradients across the shock as shown in Eq. (2.15). The equations for the generation of the coordinate system (Eqs. (2.9), (2.10)), using coordinate control, were solved, as well as the Navier-Stokes equations, when a quasi steady-state has been reached. This process was repeated after a pre-assigned number of time steps, usually 40. Thus the coordinate system was refined in the region of the shock and moved with it. This measure reduced the need of having a very refined mesh in the entire computational domain by providing refinement only in the region through which the shock happened to be passing at any given time. However, it must be noted that this refinement near the shock was achieved at the expense of the accuracy near the wall where coordinate contraction is always needed to resolve the boundary layer.

## 5. Technique of Numerical Solution

The first step in the numerical solution of the transformed N-S equations is the determination of the computational domain so that the appropriate boundary conditions may be prescribed around it. In the present case of supersonic flow, the flow field remains unperturbed upstream of the bow shock wave, and the computational domain is limited upstream by a boundary located at a short distance ahead of the bow shock. The "stand-off" distance of this detached shock, for a given freestream Mach number, is estimated using empirical equations [ 7 ]. On the upstream boundary the uniform flow conditions were used as boundary conditions. Particular care had to be taken to ensure that the bow shock did not cut across any segment of this upstream boundary. On the downstream boundary the boundary conditions varied with time and were determined by solving the Euler's equations (cf. Section 4).

The computational domain and the profile of the body in it having been determined, the next step was the numerical generation of the coordinate system which has already been described. The cartesian coordinates of each of the mesh points in the entire computational domain having been determined and stored, the coefficients that occur in the Navier-Stokes equations due to transforming them into general curvilinear coordinates could now be calculated and stored in a file.

The actual solution of the N-S equations now starts with an assumed initial guess of the solution for the entire computational domain. These initial conditions need not necessarily be physically realistic and when they are not, the transient solution has no physical meaning. In the present case the initial conditions chosen for the whole flow field were the uniform flow conditions that were prescribed on the upstream boundary. It was however found that this could not be done if the freestream Mach

number was very high, or if the isothermal temperature condition prescribed on the body was far different from the freestream value. The finite-difference scheme chosen was the S.O.R. which is an implicit scheme. The value of the optimum acceleration parameter for all the equations, i.e., continuity, momentum and energy, was determined, by trial, to be 0.9. In approximating the convective derivatives of these equations, the average of the product (A.O.P.) finite-difference scheme rather than the product of the average (P.O.A.), proved fruitful, eventhough it is generally considered that a non-linear instability can result in regions of flow reversal when the average of the product scheme is used.

The problem of the treatment of boundary conditions at an impermeable wall in viscous compressible flows reduces to that of the calculation of the pressure or of the density. In this research the wall density was calculated from the continuity equation written at the wall. Peyret and Viviand [1 ] report that such a technique is of delicate use and may lead to strong oscillations or even to divergence if no artificial viscosity term is added to the continuity equation; and that, in particular, in the case of separated flows negative values of the density may be obtained. This, in fact, was what happened at the trailing-edge point using the continuity equation. This problem was overcome by using an explicit discretization based on the leap-frog scheme, only at the trailing edge (cf. Eq. 4.23).

In general it was found that at a given time-step iterative convergence to the tolerance of $10^{-6}$ occurred in about 7 iterations. While carrying out these iterations the downstream boundary conditions varied with every iteration. Progress in time was made by increasing the time interval $\Delta t$ by .01 at the end of each time step. The problem of wiggles was overcome

by applying the Shuman filter at the end of every 5 time steps. Provision was made in the computer program to store the solution obtained at the end of any desired time step in a file; and the ability to read back from this storage file and to restart the program where it last left off was also incorporated. The computer program also locates and calculates the maximum change that occurs in a typical flow variable, such as density, along every $\xi$ = constant line that passes through the region of the shock. Thus at the end of any desired time step the location of the shock and the change in the density across it is automatically recorded. This information is used again if necessary in the generation of a new coordinate system wherein the coordinate attraction technique is used to refine the mesh in the immediate vicinity of the shock.

On an average it took 0.525 minutes of computer time (on a UNIVAC 1106) to achieve iterative convergence at each time step. The stand-off distance of the bow-shock became quite constant after about 320 time steps each increment in time-step being equal to .01. All the programs were, however, run up to 400 time steps and the total computer time requirement to achieve this "steady-state" solution was about 2 hours and 30 minutes.

5.1. Discussion of Results:

The numerical solution of the complete Navier-Stokes Equations for a supersonic flow was obtained for the flow about a two-dimensional circular cylinder. The uniform flow conditions used in the computations were $M_\infty = 4.6$, $Re_\infty = 10{,}000$, $T^*_\infty = 167°K$, $p^*_\infty = 14.93\ N/M^2$ and $P_r = 0.72$. For these free-stream conditions the coefficient of viscosity works out to be $\mu^*_\infty = 1.13154 \times 10^{-5}$ kg/m-sec and the density $\rho^*_\infty = 3.11593 \times 10^{-4}\ kg/m^3$. The ratio of the specific heats was assumed to be $\gamma = 1.40$. All calculations

presented in this report have been performed for the isothermal wall temperature $T_w^*$ of 556°K. The diameter of the circular cylinder was $2R_n^* = 0.3048$m. The Knudsen number for a perfect gas is defined by the expression $\sqrt{\gamma\pi/2}\ (M_\infty/Re_\infty)$, which for the above free-stream conditions is $6.821529 \times 10^{-4}$.

The graphical results presented correspond to the steady state solutions at a characteristic time of 3.20, with the exception of the Mach contour plots which are presented at two periods of time so as to give an insight into the formation and progress of the bow shock wave as the solution of the N-S Equations advances in time towards a steady state.

Figure 3 shows the physical field, which constituted the computational domain and Figure 4 represents the transformed $\xi$-$\eta$ field used in the numerical computations. A fairly compact field with 39 lines in the $\xi$-direction and 35 lines in the $\eta$-direction was used. Even so the computer program required 62K of core capacity on a UNIVAC 1100 series computer.

Figures 7a-b are the Mach contour plots at the characteristic times of 0.8, and 3.2, and depict the progression of the bow shock wave from the body to its steady state stand-off distance. The Mach contour interval is 0.1. The sonic lines between the bow shock and the body, in which region the flow is wholly subsonic, are indicated in Figure 7b. It can be seen from this figure that aft of the body too, a subsonic region exists which extends up to a distance of about 2 times the diameter of the cylinder from its center. Behind this subsonic region, the flow again is supersonic. In the field shown in Figure 3, the computational domain downstream of the body was limited by a semi-circle of radius 2.5 and the boundary conditions on this exit plane, as mentioned in Sect. 4.2.4, were established by solving the Euler's Equations on it. Since the downstream boundary is located beyond the subsonic region

and wholly in a supersonic field of flow the use of the Euler's Equations is thus seen to be perfectly valid and accurate. In Figure 3 it can be noticed that the upstream boundary of the field starts and ends vertically above and below the cylinder respectively. This was dictated by the need of having to prescribe the free-stream conditions at least up to those points.

As the $\eta$-line spacing was already sparse to begin with, the scope for mesh refinement in the region of the shock was very much restricted. In Figure 8 the concentration of the $\eta$-lines in the region of the shock is exhibited.

Figures 9 through 12 depict the variation of density, pressure, temperature and velocity from the front stagnation point to the upstream boundary along the symmetry line (I = 20) in the steady state. Figure 9a is the density distribution without mesh refinement, while 9b is the density variation with mesh refinement in the shock region. While the trend of density, pressure, temperature and velocity distributions seems satisfactory, the shock stand-off distance is more than what the ideal theories of Refs. [6] and [7] predict. This effect is first due to the solution of the Navier-Stokes equations and second due to the introduction of numerical dissipative terms. Moreover, since the present method is designated for capturing the shock, the shock stand-off distance is not forced in advance as is the case with the shock fitting method.

Figure 13 shows the variation of the coefficient of pressure ($C_p$) along the upper half of the cylinder from the front stagnation point to the trailing edge.

Figures 14a-b show the distribution of wall densities from 0° to 90° normalized with the stagnation value without and with mesh refinement

respectively. Finally in Figure 15 the results plotted in Figure 14a are compared with the experimental results quoted in Ref. 11. It is seen that the numerical results of the Navier-Stokes equations, for the free-stream conditions considered, yields results which are quite in agreement with those obtained by experiments.

Figures 16 and 17 show the computational domain and the sensity ratios for a cylinder with aft body for $M_\infty = 4.6$ and $R_e = 10^4$.

## 6.0. CONCLUSIONS

A computer code for the numerical solution of the Navier-Stokes equations for viscous compressible flows with detached bow shocks ahead of two-dimensional arbitrary shaped bodies has been developed. The outer upstream and downstream boundaries can also be chosen arbitrarily subject to some obvious physical requirements. The numerical generation of coordinates is performed separately and then the transformed Navier-Stokes equations are solved on these coordinates.

The results reported in this paper pertain to circular cylinders with and without an aft body as body shapes. The outer boundary is formed of a hyperbolic arc on the upstream side and of a circular arc on the downstream side. An implicit finite difference scheme with point-SOR is used to solve the Navier-Stokes equations. The computational domain is comprised of 39 x 35 mesh points. Iterative convergence with a tolerance of $10^{-6}$ at each time step of $\Delta t = .01$ is obtained in about 6 iterations. The total computer time to achieve a steady state solution on the UNIVAC 1100 series computer, including the time required in the generation of curvilinear coordinates, is about 3 hours.

The method developed for the concentration of coordinates in the shock region seems to work in the sense that one or two $\eta$-lines are added to this region. However, because of the coordinate shifts, a cruder mesh spacing results in the non-shock region, which occasionally gives rise to oscillations. A better and finer coordinate spacing before the application of the mesh refinement is expected to yield better results.

## References


[1] Peyret, R., and Viviand, H., "Computation of Viscous Compressible Flows Based on the Navier-Stokes Equations," AGARD-AG-212, 1975.

[2] Rusanov, V. V., "A Blunt Body in a Supersonic Stream," Annual Review of Fluid Mechanics, Vol. 8, 1976, p. 377.

[3] Thompson, J. F., Thames, F. C., and Mastin, C. W., "Automatic Numerical Generation of Body-Fitted Curvilinear Coordinate System for Field Containing any Number of Arbitrary Two-Dimensional Bodies," Journal of Computational Physics, Vol. 15, 1974, p. 299.

[4] Thames, F. C., "Numerical Solution of the Incompressible Navier-Stokes Equations about Arbitrary Two-Dimensional Bodies," Ph.D. Dissertation, Mississippi State University, 1975.

[5] Warsi, Z. U. A., and Thompson, J. F., "Machine Solutions of Partial Differential Equations in the Numerically Generated Coordinate Systems," Mississippi State University, Aerophysics and Aerospace Engineering, Rep. No. MSSU-EIRS-ASE-77-1, August 1976.

[6] Van Dyke, M. D. and Gordon, H. D., "Supersonic Flow Past a Family of Blunt Axisymmetric Bobies," NASA Tech. Rep. R-1, 1959.

[7] Billig, F. S., "Shock-Wave Shapes Around Spherical-and Cylinderical-Nosed Bodies," J. Spacecraft, Vol. 4, No. 6, 1967, p. 822.

[8] MacCormack, R. W., "Numerical Solution of the Interaction of a Shock Wave with a Laminar Boundary Layer," Lecture Notes in Physics," Springer-Verlag, Berlin, New York, Vol. 8, 1972, p. 151.

[9] Boris, J. P., and Book, D. L., "Flux-Corrected Transport. 1. SHASTA, A Fluid Transport Algorithm that Works," Journal of Computational Physics, Vol. 11, 1973, p. 38.

[10] Vliegenthart, A. C., "The Shuman Filtering Operation and the Numerical Computation of Shock Waves," Journal of Engineering Science, Vol. 4, 1970, p. 341.

[11] Tannehill, J. C., Holst, T. L., and Rakich, J. V., "Numerical Computation of Two-Dimensional Viscous Blunt Body Flows with an Impinging Shock," AIAA J., Vol. 14, No. 2, 1976, p. 204.

[12] Winslow, A. J., "Numerical Solution of the Quasi-Linear Poisson Equation in a Non-Uniform Triangular Mesh," Journal of Computational Physics, Vol. 2, 1966, p. 149.

[13] Barfield, W. D., "An Optimal Mesh Generator for Lagrangian Hydrodynamic Calculations in Two Space Dimensions," Journal of Computational Physics, Vol. 6, 1970, p. 417.

[14] Chu, W. H., "Development of a General Finite Difference Approximation for a General Domain, Part I: Machine Transformation," Journal of Computational Physics, Vol. 8, 1971, p. 392.

[15] Amsden, A. A. and Hirt, C. W., "A Simple Scheme for Generating General Curvilinear Grids," Journal of Computational Physics, Vol. 11, 1973, p. 348.

[16] Godunov, S. K. and Prokopov, G. P., "The Use of Moving Meshes in Gas Dynamics Computation," USSR Computational Mathematics and Mathematical Physics, Vol. 12, 1972, p. 182.

[17] Thames, F. C., Thompson, J. F., and Mastin, C. W., "Numerical Solution of the Navier-Stokes Equations for Arbitrary Two-Dimensional Airfoils," Proceedings of NASA Conference on Aerodynamic Analyses Requiring Advanced Computers, Langley Research Center, NASA SP-347, 1975.

[18] Thompson, J. F., Thames, F. C., Mastin, C. W., and Shanks, S. P., "Numerical Solutions of the Unsteady Navier-Stokes Equations for Arbitrary Bodies Using Boundary-Fitted Curvilinear Coordinates," Proceedings of Arizona/AFOSR Symposium on Unsteady Aerodynamics, Univ. of Arizona, Tucson, Arizona, 1975.

[19] Thompson, J. F., Thames, F. C., and Shanks, S. P., "Use of Numerically Generated Body-Fitted Coordinate Systems for Solution of the Navier-Stokes Equations," Proceedings of AIAA 2nd Computational Fluid Dynamics Conference, Hartford, Connecticut, 1975.

[20] Thompson, J. F., Thames, F. C., and Mastin, C. W., "Boundary-Fitted Curvilinear Coordinate Systems for Solution of Partial Differential Equations on Fields Containing any Number of Arbitrary Two-Dimensional Bodies," NASA Contractor's Report, NASA CR-2729, July 1977.

[21] Devarayalu, K., "Numerical Solution of the Navier-Stokes Equations for Supersonic Flows with Strong Shocks," Ph.D. Dissertation, August 1978.

[22] Harten, A., and Zwas, G., "Switched Numerical Shuman Filters for Shock Calculations," Journal of Engineering Mathematics, Vol. 6, No. 2, 1972, p. 207.

[23] Spain, B., "Tensor Calculus," Oliver and Boyd, New York: Interscience Publishers, Inc., 1953, p. 29.

[24] Warsi, Z. U. A., "A Course of Lectures on the Theoretical Aspects of Laminar Viscous Incompressible Flows," published by the Department of Aerophysics and Aerospace Engineering, Mississippi State University, October 1975.

[25] Roache, P. J., "Computational Fluid Dynamics," Hermosa Publishers, 1972, p. 165.

## Appendix A

This Appendix summarizes the basic rules of tensor calculus [23], [24] used in transforming Eqs. (3.1) - (3.3), and the expanded form of the pertinent terms which appear in Eqs. (3.17) - (3.20). In all the formulae given below, repeated indices imply summation.

Let $x_i$ be the Cartesian coordinates and $\xi^i$ the general curvilinear coordinates. Then the metric coefficients are

$$g_{ij} = \frac{\partial x_k}{\partial \xi^i} \frac{\partial x_k}{\partial \xi^j} \tag{A-1}$$

$$g^{ij} = \frac{\partial \xi^i}{\partial x_k} \frac{\partial \xi^j}{\partial x_k} \tag{A-2}$$

$$g^{ik} g_{jk} = \delta^i_j \tag{A-3}$$

$$g = \det\ (g_{ij}) \tag{A-4}$$

$$J = \sqrt{g} = \frac{\partial(x_1, x_2, x_3)}{\partial(\xi^1, \xi^2, \xi^3)} \tag{A-5}$$

The element of length ds is given by

$$\begin{aligned} (ds)^2 &= \delta_{ij}\ dx_i\ dx_j \\ &= g_{ij}\ d\xi^i\ d\xi^j \end{aligned} \tag{A-6}$$

Based on the above definitions, we collect other formulae from tensor calculus.

Christoffel symbols:

$$\Gamma^i_{jk} = \frac{1}{2}\ g^{i\ell}\ \left(\frac{\partial g_{\ell j}}{\partial x^k} + \frac{\partial g_{\ell k}}{\partial \xi^j} - \frac{\partial g_{jk}}{\partial \xi^\ell}\right) \tag{A-7}$$

which is symmetric in j,k. Contracting the i and j indices, we have

$$\Gamma^k_{kr} = \frac{1}{2g} \frac{\partial g}{\partial \xi^r} \tag{A-8}$$

Covariant Derivative:

$$v^i_{,k} = \frac{\partial v^i}{\partial \xi^k} + \Gamma^i_{kr} \, v^r \tag{A-9}$$

Divergence of A Vector:

$$\text{div } \underset{\sim}{v} = \frac{1}{\sqrt{g}} \frac{\partial}{\partial \xi^i} (\sqrt{g} \, v^i) \tag{A-10}$$

Divergence of A Tensor Yielding Contravariant Components:

$$(\text{div } \tilde{\tau})^i = \frac{1}{\sqrt{g}} \frac{\partial}{\partial \xi^k} (\sqrt{g} \, \tau^{ik}) + \Gamma^i_{rs} \, \tau^{rs} \tag{A-11}$$

Laplacian of A Scalar $\phi$:

$$\nabla^2 \phi = \frac{1}{\sqrt{g}} \frac{\partial}{\partial \xi^i} (\sqrt{g} \, g^{ik} \frac{\partial \phi}{\partial \xi^k}) \tag{A-12}$$

The transformation of Eqs. (3.1) - (3.3) is now direct. Using contravariant components, Eq. (3.1) becomes

$$\frac{\partial \rho}{\partial t} + \frac{1}{\sqrt{g}} \frac{\partial}{\partial \xi^i} (\rho \sqrt{g} \, v^i) = 0 \tag{A-13}$$

Equation (3.2) becomes

$$\frac{\partial}{\partial t} (\rho v^i) + \frac{1}{\sqrt{g}} \frac{\partial}{\partial \xi^k} (\sqrt{g} \, \tau^{ik}) + \Gamma^i_{rs} \, \tau^{rs} = 0 \tag{A-14}$$

where i = 1,2 for two dimensions.

Equation (3.3) becomes

$$\frac{\partial \Psi}{\partial t} + \frac{1}{\sqrt{g}} \frac{\partial}{\partial \xi^i} (\rho \sqrt{g} \, b^i) = 0 \tag{A-15}$$

The expanded form of these equations are Eqs. (3.11) - (3.13).

The terms appearing in Eqs. (3.17) - (3.20) are

$$\theta = \frac{1}{g}\left(g_{12}\frac{\partial P}{\partial \eta} - g_{22}\frac{\partial P}{\partial \xi}\right) + \frac{P}{g}\{g_{22}\,(\Gamma^1_{11} + \Gamma^2_{12})$$

$$- g_{12}\,(\Gamma^1_{12} + \Gamma^2_{22})\} + \frac{\varepsilon}{\sqrt{g}}\left(g_{22}\frac{\partial K}{\partial \xi} - g_{12}\frac{\partial K}{\partial \eta}\right)$$

$$+ \varepsilon\left(\frac{\partial D^{11}}{\partial \xi} + \frac{\partial D^{12}}{\partial \eta} + \Gamma^1_{11}\,D^{11} + 2\Gamma^1_{12}\,D^{12} + \Gamma^1_{22}D^{22}\right) \qquad \text{(A-16)}$$

$$\phi = \frac{1}{g}\left(g_{12}\frac{\partial P}{\partial \xi} - g_{11}\frac{\partial P}{\partial \eta}\right) + \frac{P}{g}\{g_{11}\,(\Gamma^1_{12} + \Gamma^2_{22})$$

$$- g_{12}\,(\Gamma^1_{11} + \Gamma^2_{12})\} + \frac{\varepsilon}{\sqrt{g}}\left(g_{11}\frac{\partial K}{\partial \eta} - g_{12}\frac{\partial K}{\partial \xi}\right)$$

$$+ \varepsilon\left(\frac{\partial D^{12}}{\partial \xi} + \frac{\partial D^{22}}{\partial \eta} + \Gamma^2_{11}\,D^{11} + 2\Gamma^2_{12}\,D^{12} + \Gamma^2_{22}\,D^{22}\right) \qquad \text{(A-17)}$$

$$\psi = \varepsilon\left\{\frac{\partial}{\partial \xi}\left(\sqrt{g}\,\nu^1\right) + \frac{\partial}{\partial \eta}\left(\sqrt{g}\,\nu^2\right)\right.$$

$$+ \alpha_o\frac{\partial}{\partial \xi}\left\{\frac{\mu}{\sqrt{g}}\left(g_{22}\frac{\partial T}{\partial \xi} - g_{12}\frac{\partial T}{\partial \eta}\right)\right\}$$

$$+ \alpha_o\frac{\partial}{\partial \eta}\left\{\frac{\mu}{\sqrt{g}}\left(g_{11}\frac{\partial T}{\partial \eta} - g_{12}\frac{\partial T}{\partial \xi}\right)\right\} \qquad \text{(A-18)}$$

Defining

$$G_{ij} = g_{ij}/\sqrt{g} \qquad \text{(A-19)}$$

the terms $D^{11}$, $D^{12}$, . . . , $\nu^1$, $\nu^2$, etc., are

$$D^{11} = 2\mu[G_{22}\,u_\xi - G_{12}\,u_\eta + (G_{22}\,\Gamma^1_{11} - G_{12}\,\Gamma^1_{12})u$$

$$+ (G_{22}\,\Gamma^1_{12} - G_{12}\,\Gamma^1_{22})v] \qquad \text{(A-20)}$$

$$D^{12} = \mu[(G_{11}\ u_\eta + G_{22}\ v_\xi) - G_{12}\ (u_\xi + v_\eta)$$

$$+ \{G_{22}\ \Gamma^2_{11} + G_{11}\ \Gamma^1_{12} - G_{12}\ (\Gamma^1_{11} + \Gamma^2_{12})\}u$$

$$+ \{G_{22}\ \Gamma^2_{12} + G_{11}\ \Gamma^1_{22} - G_{12}\ (\Gamma^1_{12} + \Gamma^2_{22})\}v] \qquad \text{(A-21)}$$

$$D^{22} = 2\mu[G_{11}\ v_\eta - G_{12}\ v_\xi + (G_{11}\ \Gamma^2_{12} - G_{12}\ \Gamma^2_{11})u$$

$$+ (G_{11}\ \Gamma^2_{22} - G_{12}\ \Gamma^2_{12})v] \qquad \text{(A-22)}$$

$$K = \lambda\ [u_\xi + v_\eta + (\Gamma^1_{11} + \Gamma^2_{12})u + (\Gamma^1_{12} + \Gamma^2_{22})v] \qquad \text{(A-23)}$$

$$\nu^1 = Ku + \mu(G_{11}\ G_{22}\ u + G_{12}\ G_{22}\ v + u)v^1_{,1}$$

$$+ \mu\{G_{12}\ G_{22}\ u + (G_{22})^2 v\}v^2_{,1} - \mu\{G_{11}\ G_{12}\ u + (G_{12})^2 v - v\}v^1_{,2}$$

$$- \mu\{(G_{12})^2 u + G_{11}\ G_{22}\ v\}v^2_{,2} \qquad \text{(A-24)}$$

$$\nu^2 = Kv - \mu\{G_{11}\ G_{12}\ u + (G_{12})^2 v\}v^1_{,1}$$

$$- \mu\{(G_{12})^2 u + G_{12}\ G_{22}\ v - u\}v^2_{,1}$$

$$+ \mu\{(G_{11})^2 u + G_{11}\ G_{12}\ v\}v^1_{,2}$$

$$+ \mu\{G_{11}\ G_{12}\ u + G_{11}\ G_{22}\ v + v\}v^2_{,2} \qquad \text{(A-25)}$$

## Appendix B

### Equation for Numerical Coordinate Generation

As in Appendix A, we shall denote the Cartesian coordinates as $x_i$ (the index i serving as a label only, having no tensorial significance) and the curvilinear coordinates either as $x^i$, or $\bar{x}^i$ or $\xi^i$.

It was mentioned in Section 2 that we need formulae in which the Cartesian coordinates $x_i$ are treated as dependent variables, while the curvilinear coordinates $\xi^i$ are treated as independent variables. To achieve this goal, we shall use some formulae from general tensor calculus. In all the expressions given below, the repeated indices imply summation.

Formula for the Second Derivative:

Let $x^i$ and $\bar{x}^i$ be two general coordinate systems. The formula for the second derivative [23] is

$$\frac{\partial^2 x^r}{\partial \bar{x}^\ell \, \partial \bar{x}^m} = \bar{\Gamma}^p_{\ell m} \frac{\partial x^r}{\partial \bar{x}^p} - \Gamma^r_{ij} \frac{\partial x^i}{\partial \bar{x}^\ell} \frac{\partial x^j}{\partial \bar{x}^m} \tag{B-1}$$

where $\Gamma^i_{jk}$ and $\bar{\Gamma}^i_{jk}$ are the Christoffel symbols in the $x^i$ and $\bar{x}^i$ coordinate systems respectively. (Refer to Eq. (A-7) for definition). Since we are considering the transformation between a Cartesian and a curvilinear system, hence either $x^i$ or $\bar{x}^i$ is a Cartesian system.

If $x^r$ is a Cartesian system, then $\Gamma^r_{ij} \equiv 0$. Writing $x^r = x_r$ and $\bar{x}^i = \xi^i$, we have

$$\frac{\partial^2 x_r}{\partial \xi^\ell \, \partial \xi^m} = \Gamma^p_{\ell m} \frac{\partial x_r}{\partial \xi^p} \tag{B-2}$$

which is the formula for the second derivative of any Cartesian coordinate with respect to the curvilinear coordinates.

Next, if $\bar{x}^i$ is a Cartesian system, then $\bar{\Gamma}^p_{\ell m} = 0$. Writing $\bar{x}^i = x_i$ and $x^i = \xi^i$, we have

$$\frac{\partial^2 \xi^r}{\partial x_\ell \, \partial x_m} = - \Gamma^r_{ij} \frac{\partial \xi^i}{\partial x_\ell} \frac{\partial \xi^j}{\partial x_m} \tag{B-3}$$

which is the formula for the second derivative of any curvilinear coordinate with respect to the Cartesian coordinates.

The use of Eqs. (B-2) and (B-3) along with the equations

$$\frac{\partial \xi^i}{\partial x_\ell} = g^{ip} \frac{\partial x_\ell}{\partial \xi^p} \tag{B-4}$$

$$\frac{\partial x_r}{\partial \xi^p} \frac{\partial \xi^n}{\partial x_r} = \delta^n_p \tag{B-5}$$

yields a series of useful equations.

Inner multiplication of Eq. (B-2) with $\frac{\partial \xi^n}{\partial x_r}$ and use of Eq. (B-5) yields

$$\Gamma^r_{ij} = \frac{\partial \xi^r}{\partial x_s} \frac{\partial^2 x_s}{\partial \xi^i \, \partial \xi^j} \tag{B-6}$$

Using Eq. (B-4) in (B-7), we have

$$\Gamma^r_{ij} = g^{rt} \frac{\partial x_s}{\partial \xi^t} \frac{\partial^2 x_s}{\partial \xi^i \, \partial \xi^j} \tag{B-7}$$

Introducing Eq. (B-4) in Eq. (B-3), we have

$$\frac{\partial^2 \xi^r}{\partial x_\ell \, \partial x_m} = - \Gamma^r_{ij} \, g^{ip} \, g^{jq} \frac{\partial x_\ell}{\partial \xi^p} \frac{\partial x_m}{\partial \xi^q} \tag{B-8}$$

Another form of (B-8) can be obtained by using (B-7), which is

$$\frac{\partial^2 \xi^r}{\partial x_\ell \, \partial x_m} = - g^{rt} \, g^{ip} \, g^{jq} \frac{\partial^2 x_s}{\partial \xi^i \, \partial \xi^j} \frac{\partial x_s}{\partial \xi^t} \frac{\partial x_\ell}{\partial \xi^p} \frac{\partial x_m}{\partial \xi^q} \tag{B-9}$$

It must be noted that the right hand sides of Eqs. (B-7) - (B-9) have differentiations with respect to $\xi^i$, as desired.

Laplacian:

Setting $\ell = m$ in Eq. (B-9), using Eqs. (A-1) and (A-3), and summing over the index m, we get

$$\nabla^2 \xi^r = - g^{rt} g^{ij} \frac{\partial x_s}{\partial \xi^t} \frac{\partial^2 x_s}{\partial \xi^i \partial \xi^j} \tag{B-10}$$

In two dimensions, writing

$$\xi^1 = \xi, \ \xi^2 = \eta, \ x_1 = x, \ x_2 = y \tag{B-11}$$

and using

$$g^{11} = g_{22}/g, \ g^{12} = - g_{12}/g, \ g^{22} = g_{11}/g \tag{B-12}$$

(which are a consequence of Eq. (A-3)), we have

$$\nabla^2 \xi = [(g_{22}\, y_{\xi\xi} - 2g_{12}\, y_{\xi\eta} + g_{11}\, y_{\eta\eta})x_\eta$$

$$- (g_{22}\, x_{\xi\xi} - 2g_{12}\, x_{\xi\eta} + g_{11}\, x_{\eta\eta})y_\eta]/g^{3/2} \tag{B-13}$$

$$\nabla^2 \eta = [(g_{22}\, x_{\xi\xi} - 2g_{12}\, x_{\xi\eta} + g_{11}\, x_{\eta\eta})y_\xi$$

$$- (g_{22}\, y_{\xi\xi} - 2g_{12}\, y_{\xi\eta} + g_{11}\, y_{\eta\eta})x_\xi]/g^{3/2} \tag{B-14}$$

where

$$g = g_{11}\, g_{22} - (g_{12})^2 \tag{B-15}$$

Similarly, using (B-3) and (B-4), we easily obtain

$$\xi^r_{xy} = [\Gamma^r_{11}\, x_\eta\, y_\eta - \Gamma^r_{12}\, (x_\xi\, y_\eta + x_\eta\, y_\xi) + \Gamma^r_{22}\, x_\xi\, y_\xi]/g \tag{B-16}$$

where $\xi^1 = \xi$ and $\xi^2 = \eta$.

The Laplacian of a scalar function $f(\xi^i)$ is obtained as div (grad f),

$$\nabla^2 f = \frac{1}{\sqrt{g}} \frac{\partial}{\partial \xi^i} (\sqrt{g}\, g^{ik} \frac{\partial f}{\partial \xi^k}) \tag{B-17}$$

which in two dimensions has the form

$$\nabla^2 f = [(g_{22}\, f_{\xi\xi} - 2g_{12}\, f_{\xi\eta} + g_{11}\, f_{\eta\eta})$$

$$+ (2g_{12}\, \Gamma^1_{12} - g_{22}\, \Gamma^1_{11} - g_{11}\, \Gamma^1_{22}) f_\xi$$

$$+ (2g_{12}\, \Gamma^2_{12} - g_{22}\, \Gamma^2_{11} - g_{11}\, \Gamma^2_{22}) f_\eta]/g \qquad \text{(B-18)}$$

Unit Tangent and Normal Vectors:

In the generation of coordinates we have taken clockwise traverse along the body contour as positive. Denoting the unit tangent and normal vectors as $\underset{\sim}{t}$ and $\underset{\sim}{n}$ respectively, and $\underset{\sim}{k}$ the constant unit vector normal to the plane of the curve, the vectors ($\underset{\sim}{t}$, $\underset{\sim}{n}$, $\underset{\sim}{k}$) are assumed to form a right-handed system. The unit tangent and normal vectors for the $\xi$ = const. and $\eta$ = const. curves are

$$(\underset{\sim}{t})_{\xi = \text{const.}} = -\frac{1}{\sqrt{g_{22}}}\,(\underset{\sim}{i}x_\eta + jy_\eta) \qquad \text{(B-19)}$$

$$(\underset{\sim}{t})_{\eta = \text{const.}} = \frac{1}{\sqrt{g_{11}}}\,(\underset{\sim}{i}x_\xi + jy_\xi) \qquad \text{(B-20)}$$

$$(\underset{\sim}{n})_{\xi = \text{const.}} = \frac{1}{\sqrt{g_{22}}}\,(\underset{\sim}{i}y_\eta - jx_\eta) \qquad \text{(B-21)}$$

$$(\underset{\sim}{n})_{\eta = \text{const.}} = \frac{1}{\sqrt{g_{11}}}\,(-\,\underset{\sim}{i}y_\xi + \underset{\sim}{j}x_\xi) \qquad \text{(B-22)}$$

where $\underset{\sim}{i}$ and $\underset{\sim}{j}$ are unit vectors along x and y respectively. The resolved parts of the velocity vector along the curves $\xi$ = const. and $\eta$ = const. are

$$(\underset{\sim}{v}\cdot\underset{\sim}{t})_{\xi = \text{const.}} = -\frac{1}{\sqrt{g_{22}}}\,(ug_{12} + vg_{22}) \qquad \text{(B-23)}$$

$$(\underset{\sim}{v}\cdot\underset{\sim}{t})_\eta = \text{const.} = \frac{1}{\sqrt{g_{11}}}(ug_{11} + vg_{12}) \tag{B-24}$$

$$(\underset{\sim}{v}\cdot\underset{\sim}{n})_\xi = \text{const.} = \sqrt{\frac{g}{g_{22}}}\,u \tag{B-25}$$

$$(\underset{\sim}{v}\cdot\underset{\sim}{n})_\eta = \text{const.} = \sqrt{\frac{g}{g_{11}}}\,v \tag{B-26}$$

where u and v are the contravariant components of the velocity vector $\underset{\sim}{v}$, which are related to the Cartesian components through Eq. (3.26).

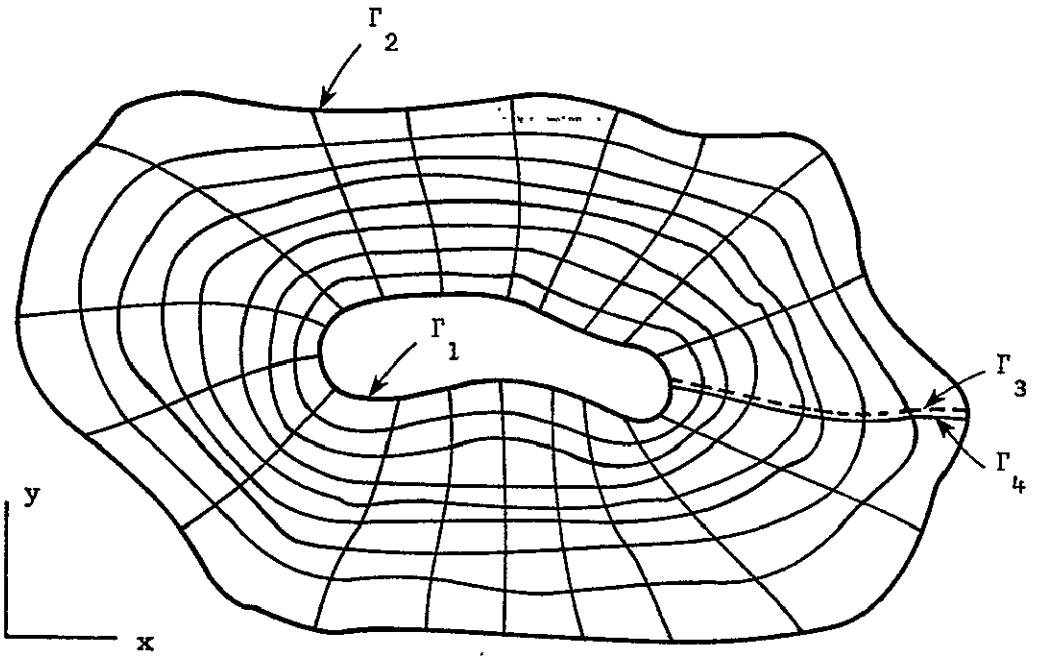


Figure 1. Physical Plane

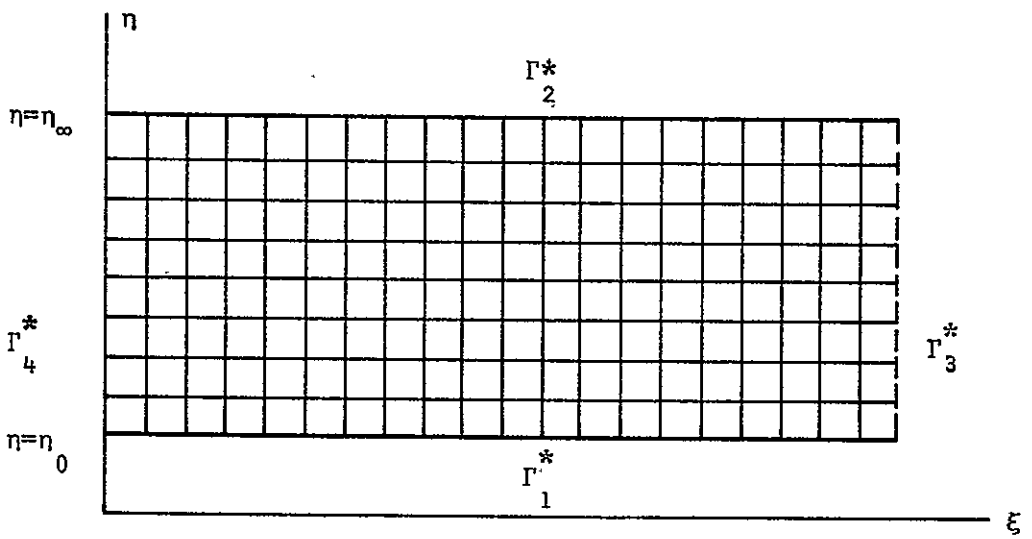


Transformed Plane
(Natural Coordinates)

Figure 2. Field Transformation

REPRODUCIBILITY OF THE
ORIGINAL PAGE IS POOR

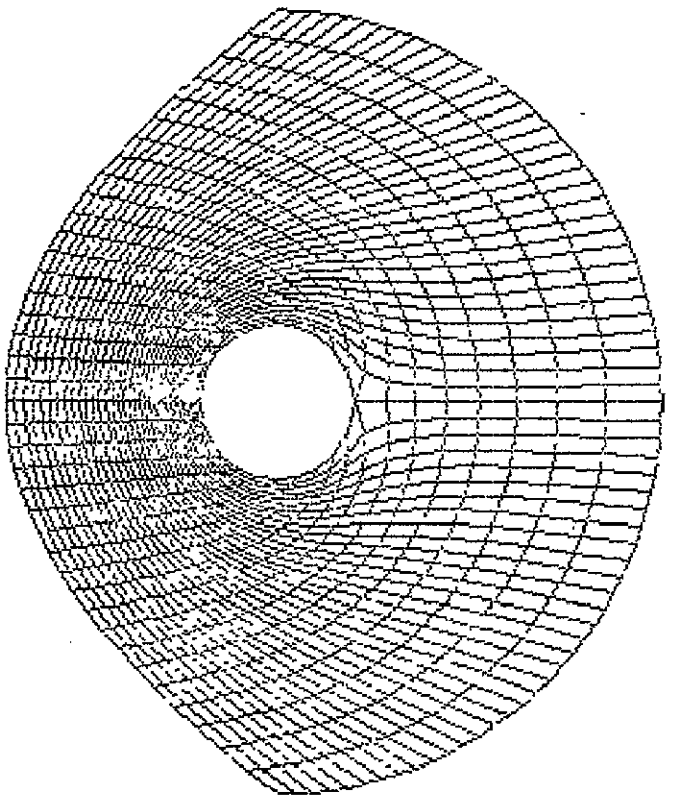

Figure 3. The Computational Domain.

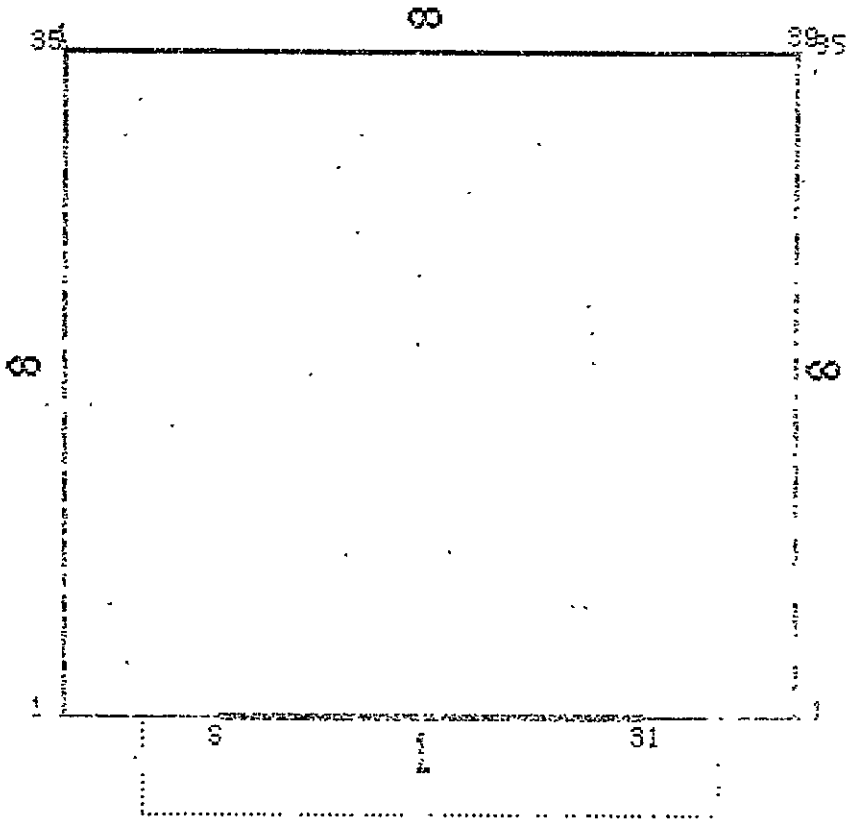


Figure 4. The Transformed Computational Domain.

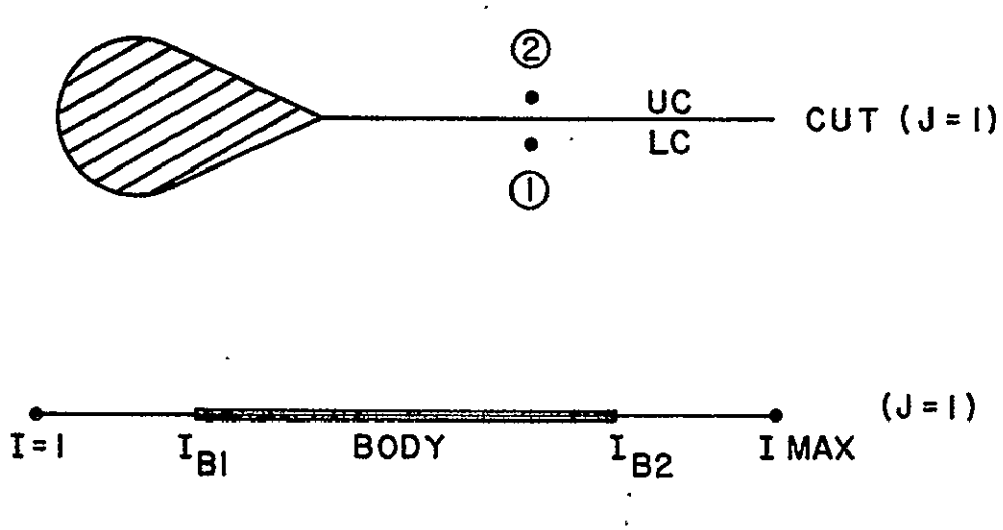


Figure 5. Grid Points Across a Cut in the Physical Plane.

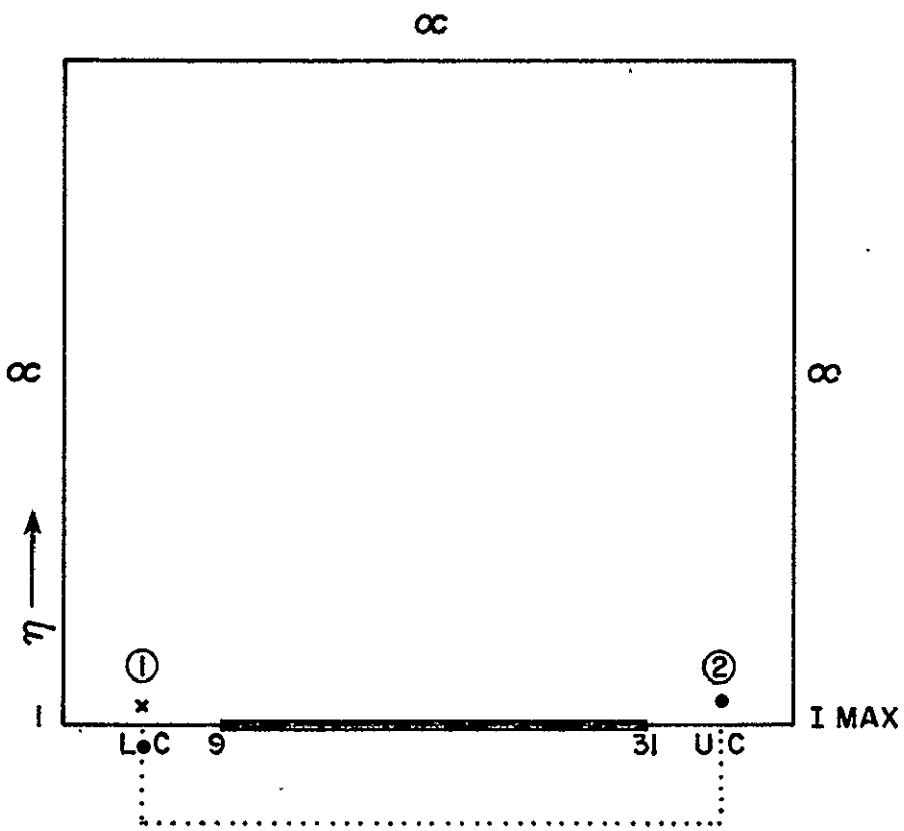


Figure 6. Grid Points Across a Cut in the Transformed Plane.

REPRODUCIBILITY OF THE
ORIGINAL PAGE IS POOR

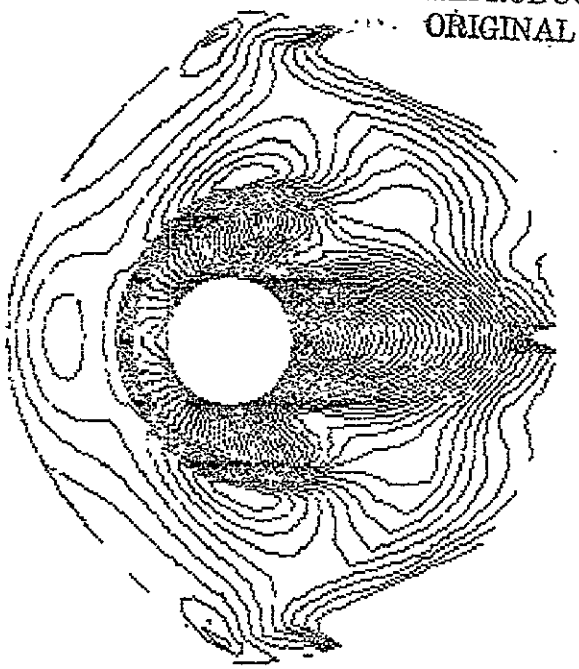

Figure 7a. Mach Contours at Time 0.8.

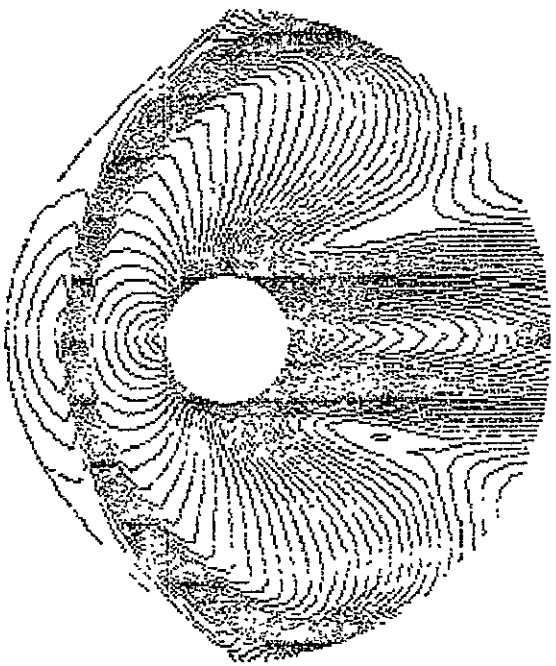

Figure 7b. Mach Contours at Time 3.2.

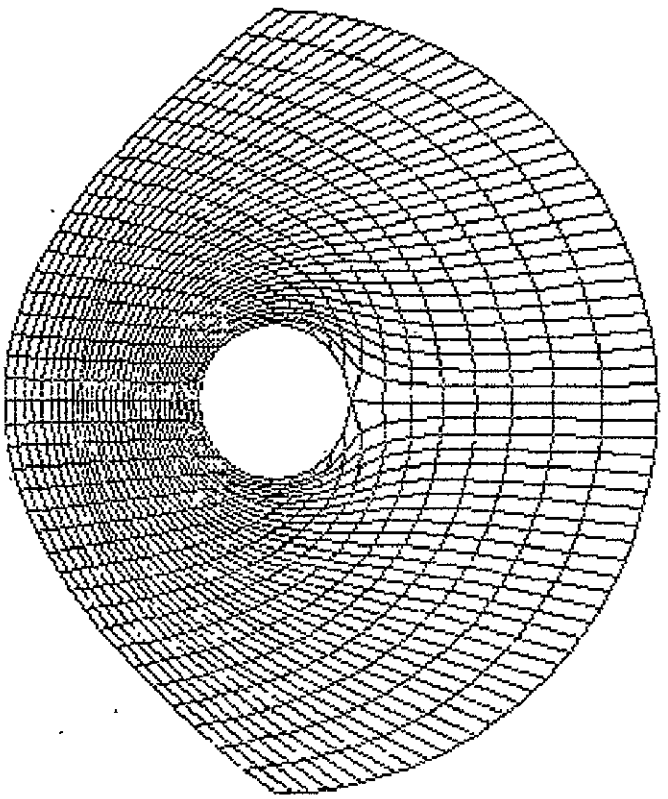

Figure 8. The Computational Domain with Mesh Refinement.

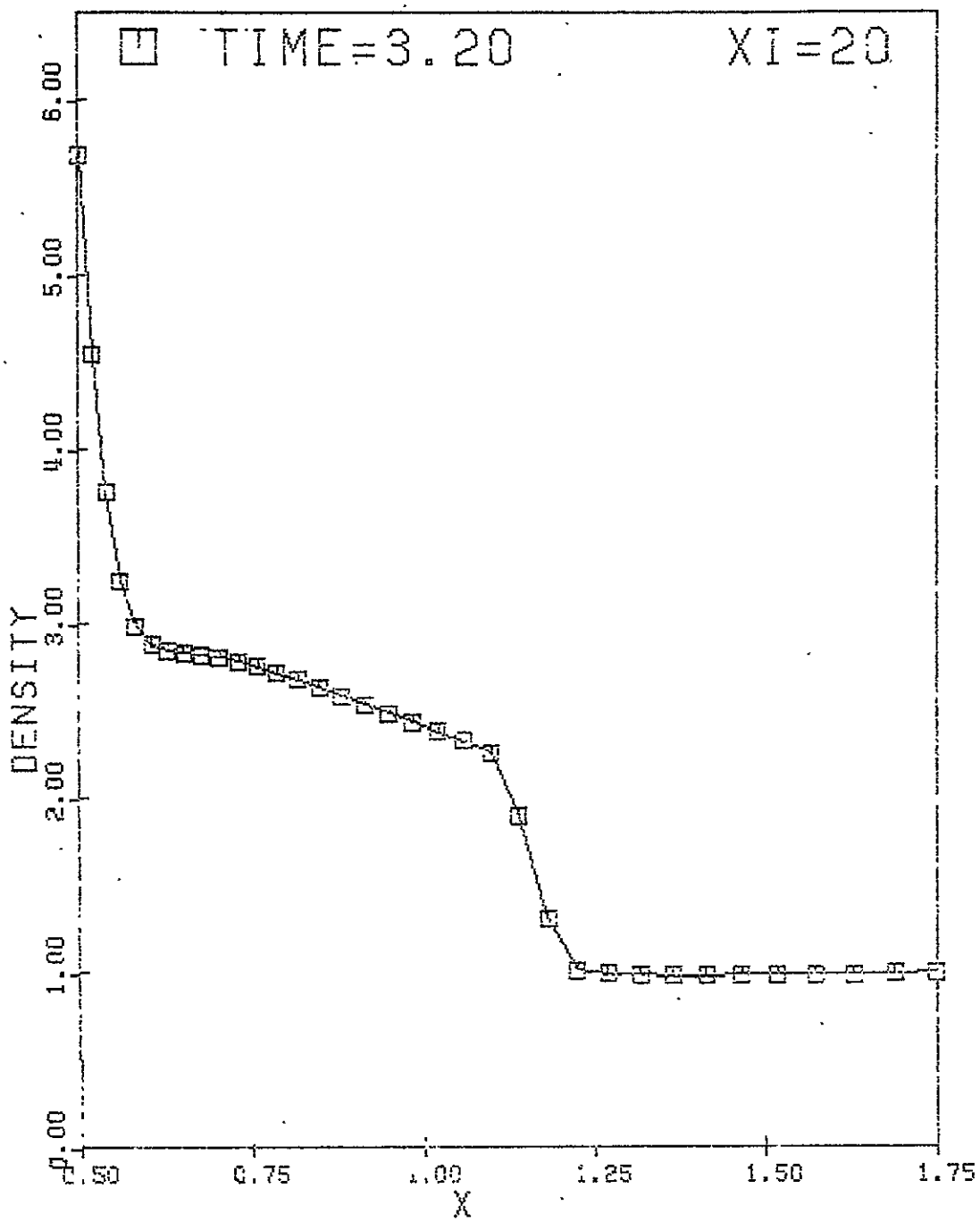


Figure 9a. Density Variation Across the Shock on Stagnation Line.

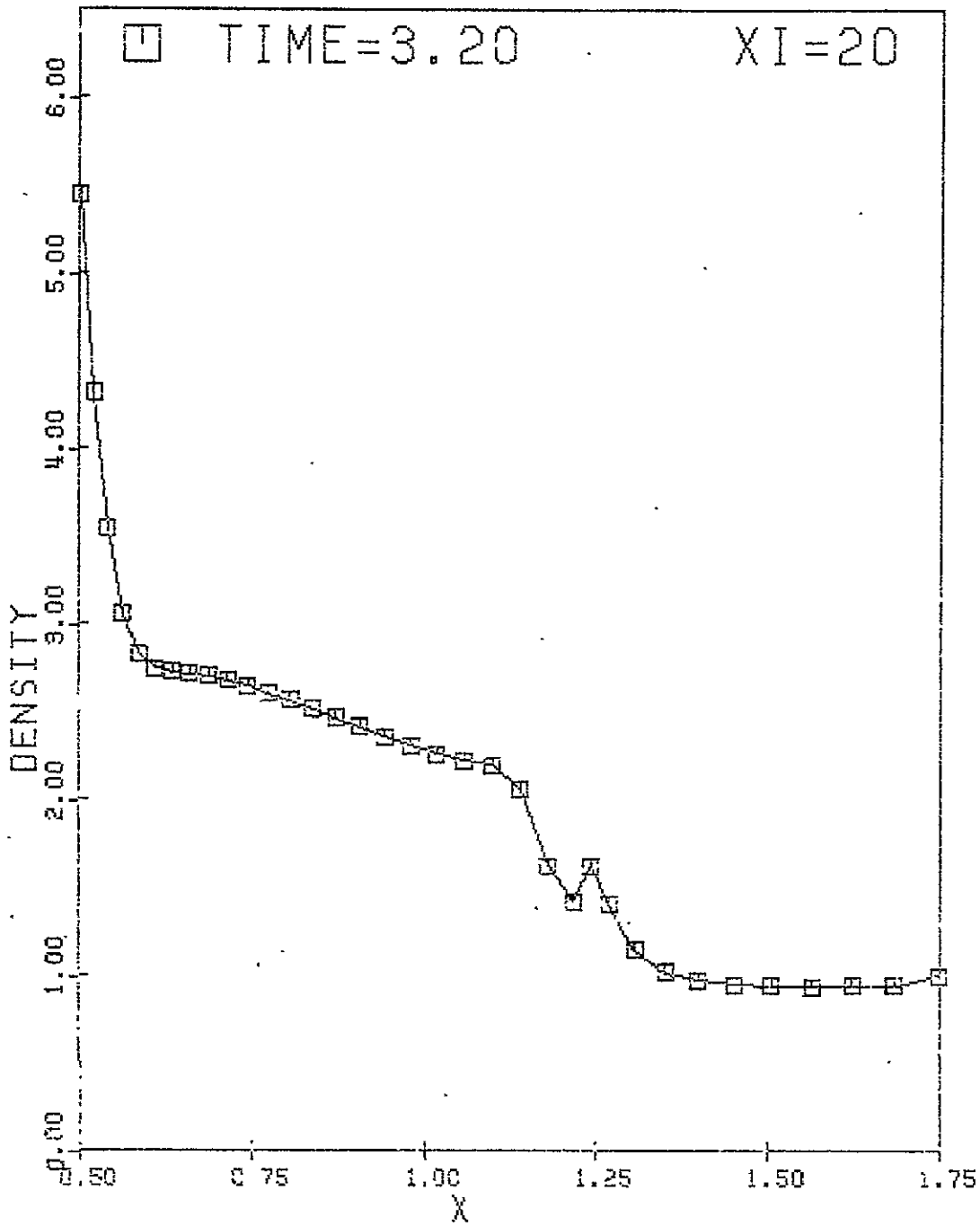


Figure 9b. Density Variation Across the Shock for Field with Mesh Refinement.

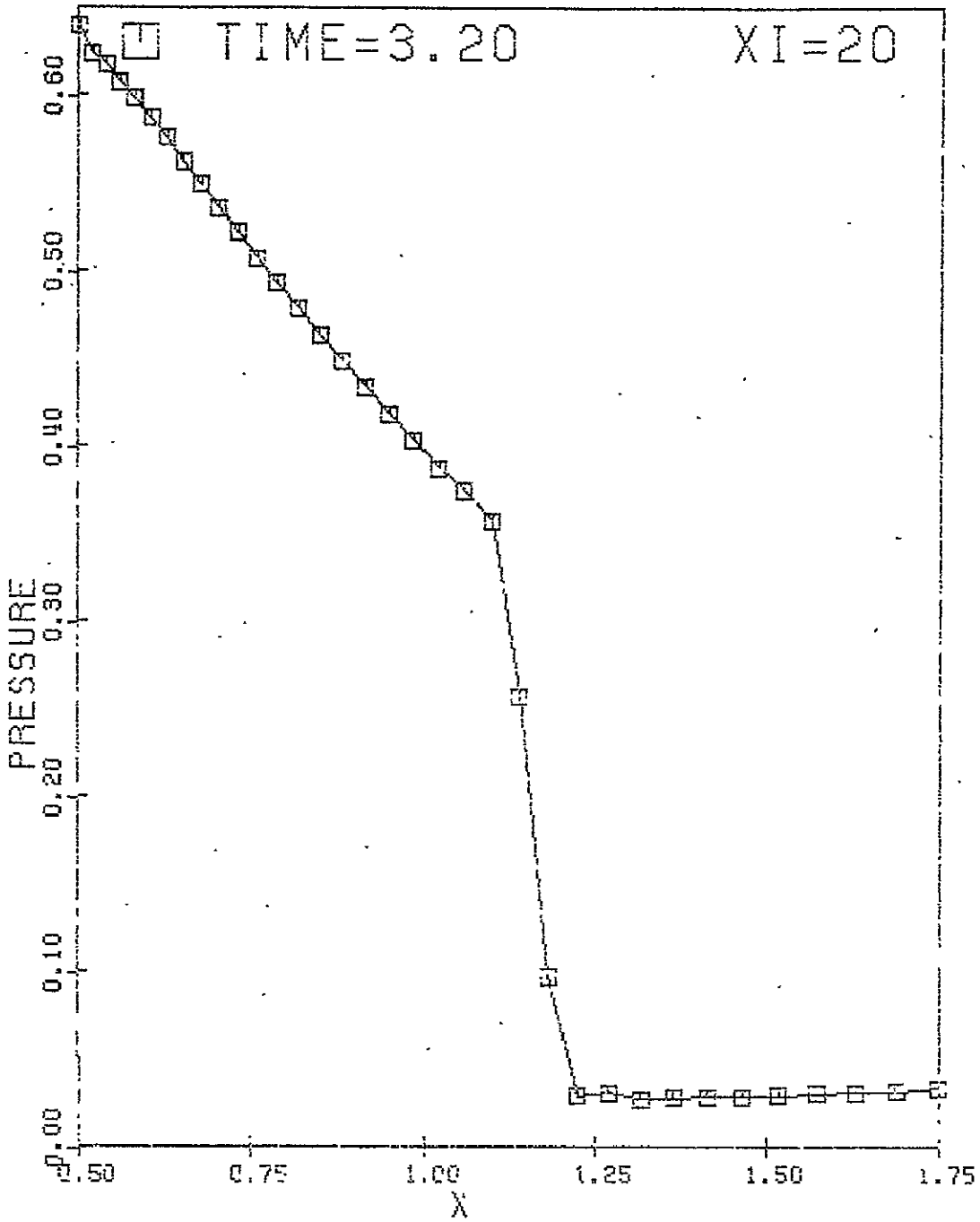


Figure 10. Pressure Variation Across the Shock on Stagnation Line.

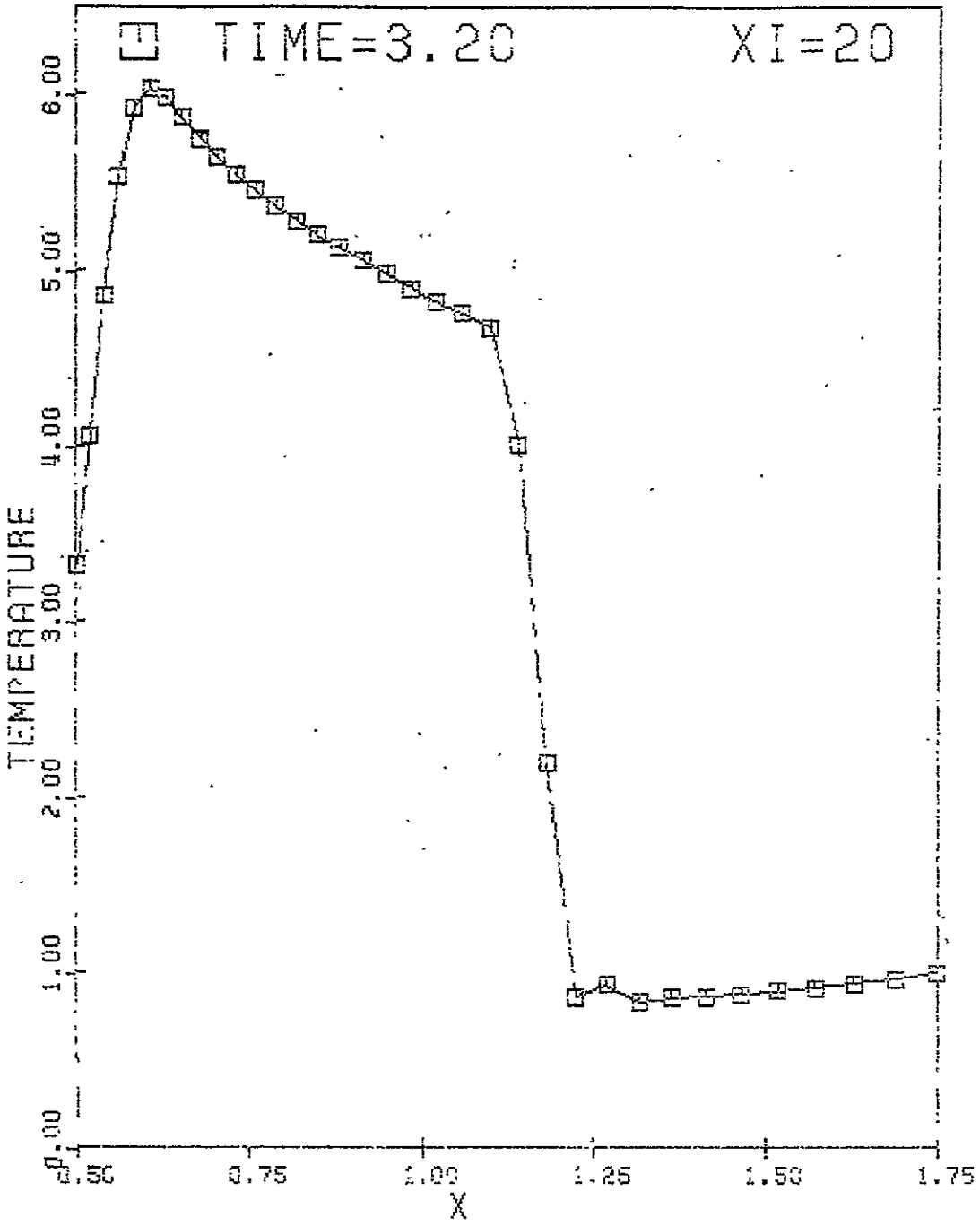


**Figure 11. Temperature Variation Across the Shock on Stagnation Line.**

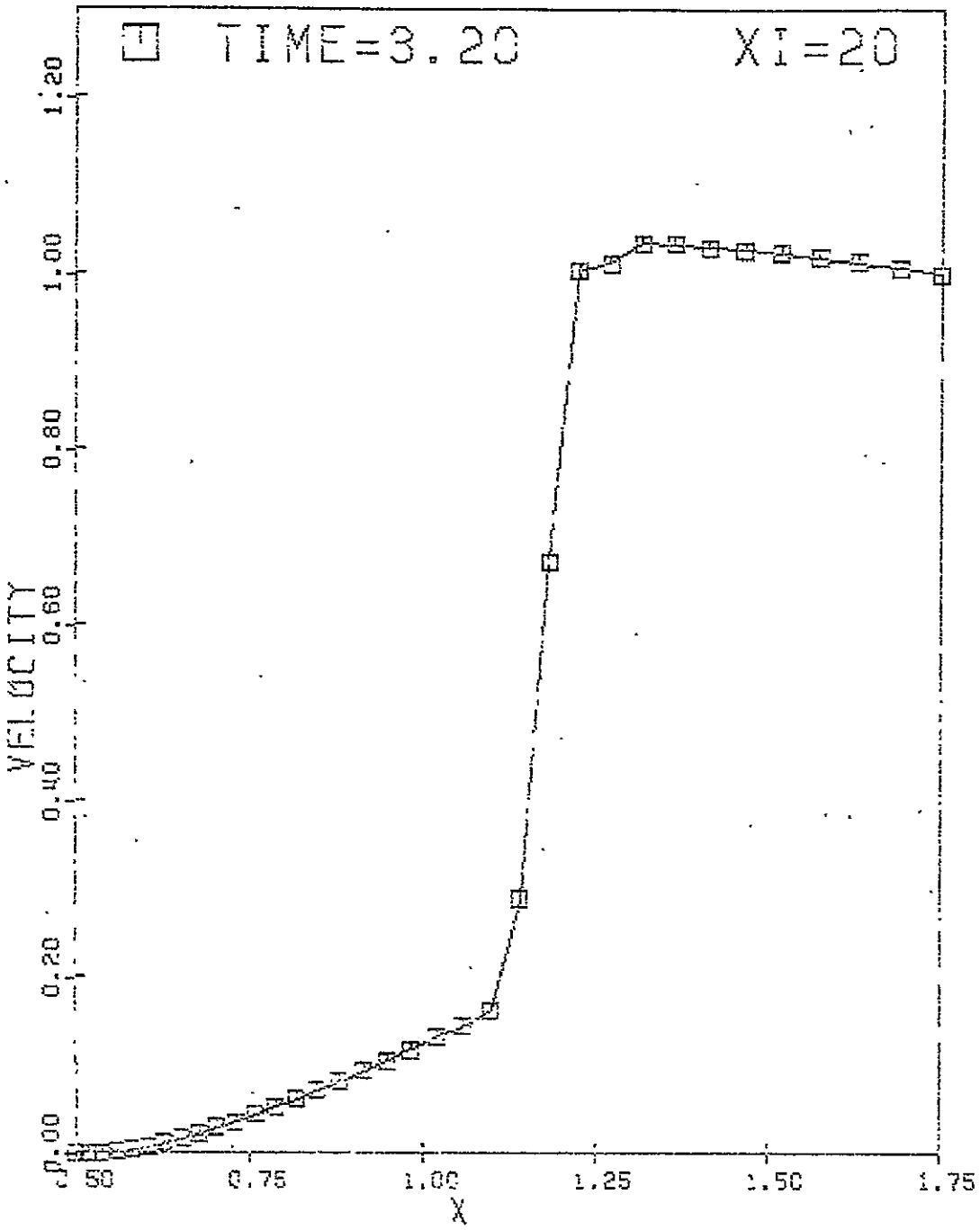


Figure 12. Velocity Variation Across the Shock on Stagnation Line.

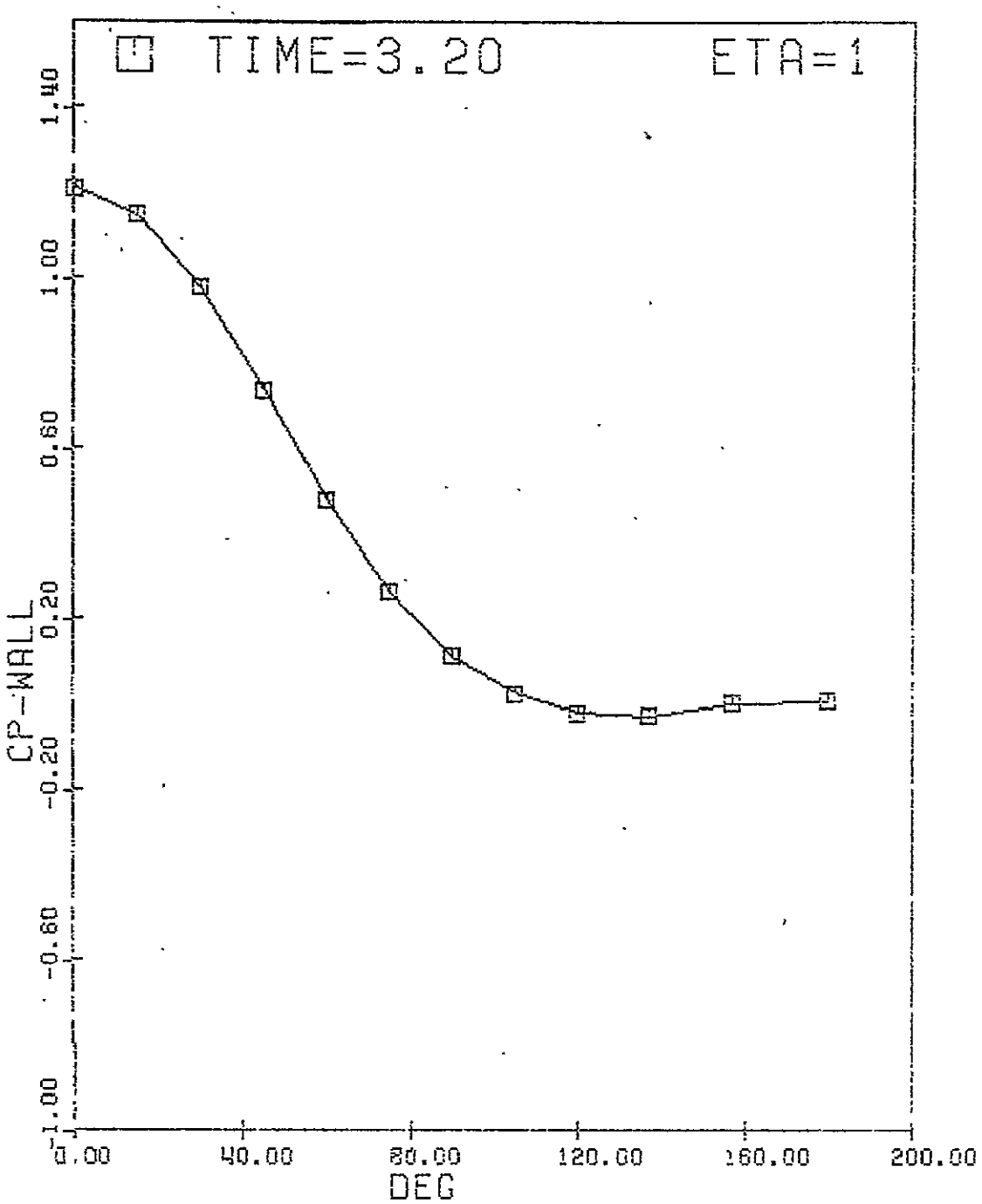


Figure 13. Coefficient of Pressure Distribution on Top of Cylinder.

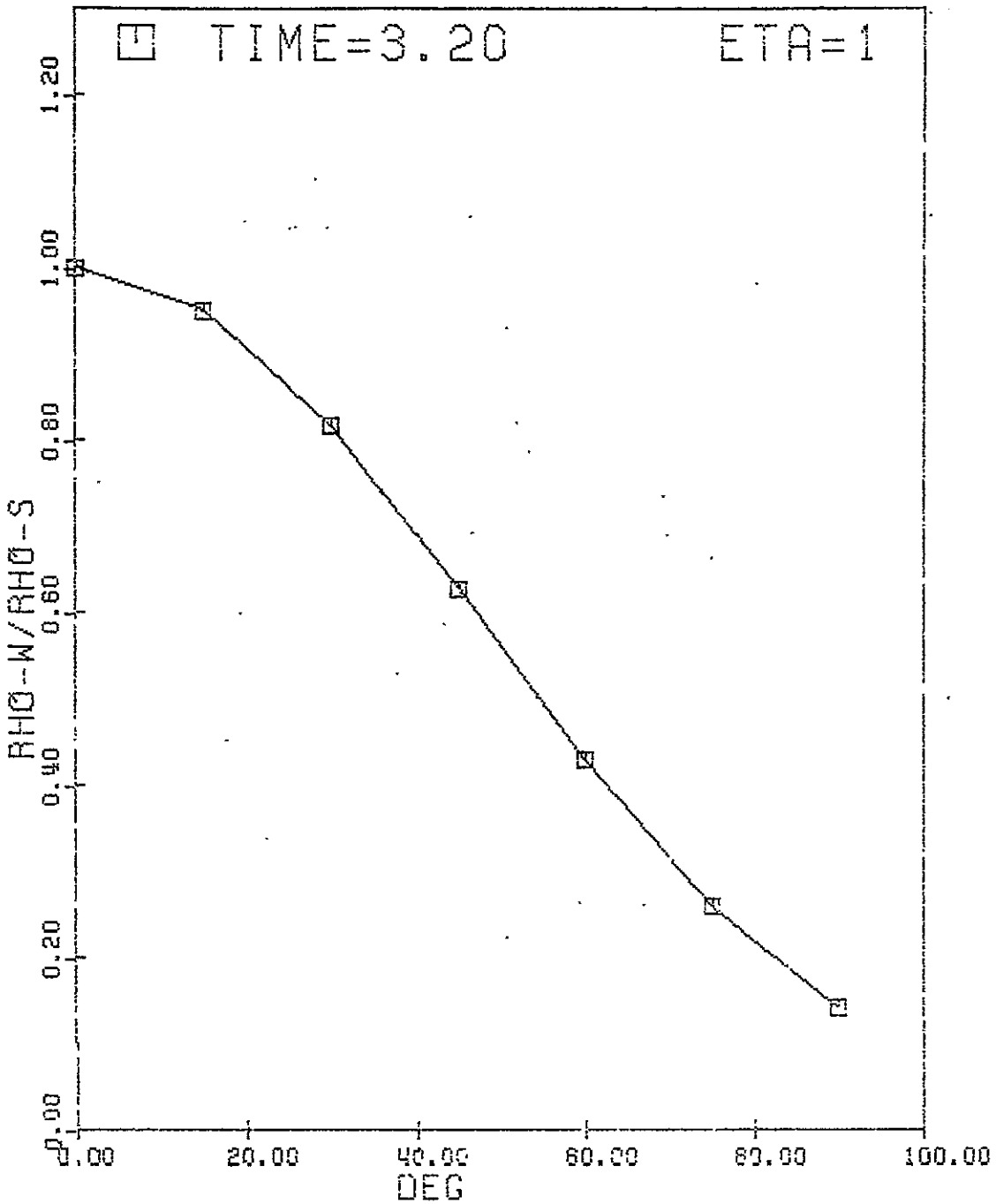


Figure 14a. Density Distribution on Cylinder from 0° to 90°.

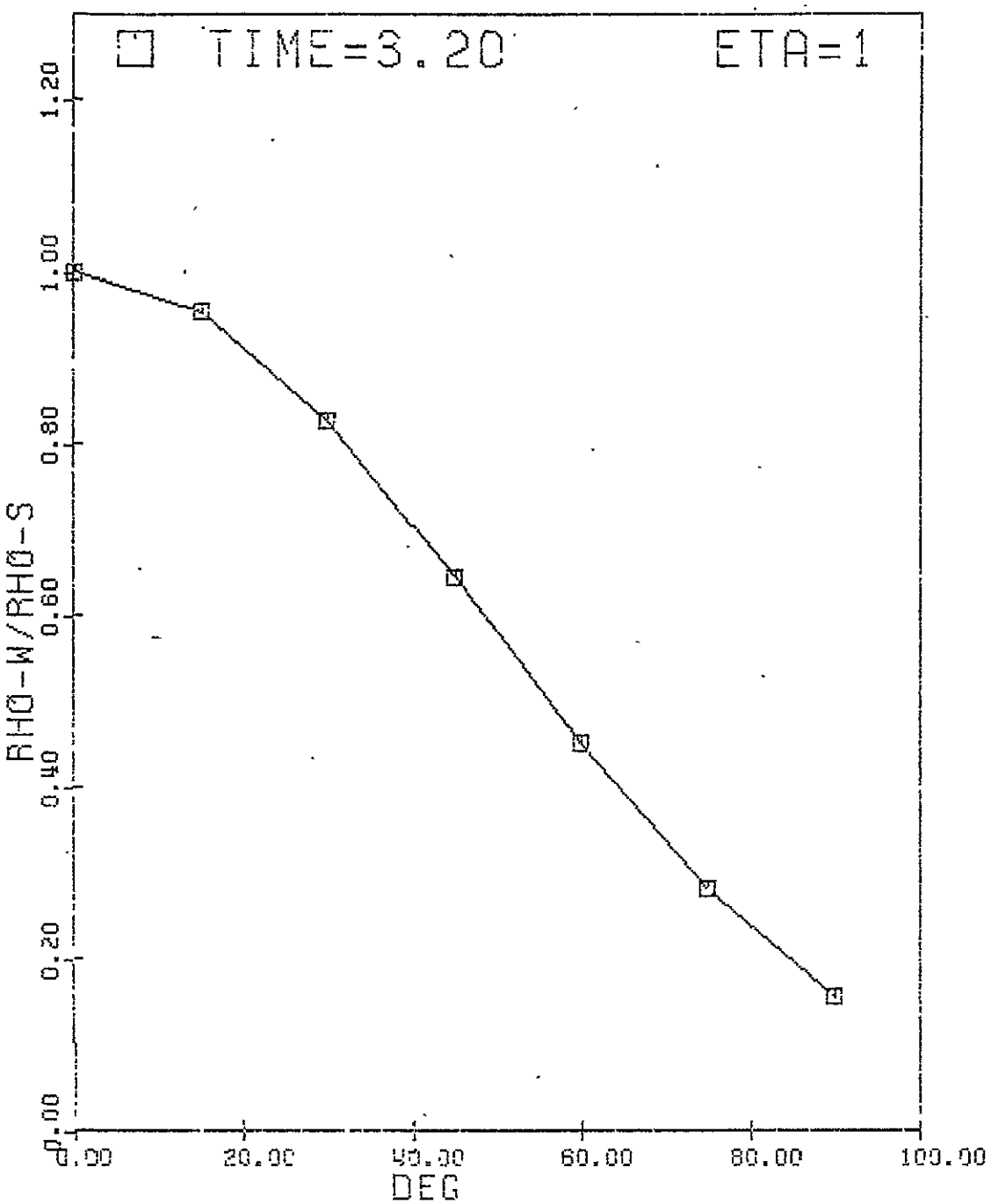


Figure 14b. Density Distribution on Cylinder from 0° to 90° for Field with Mesh Refinement.

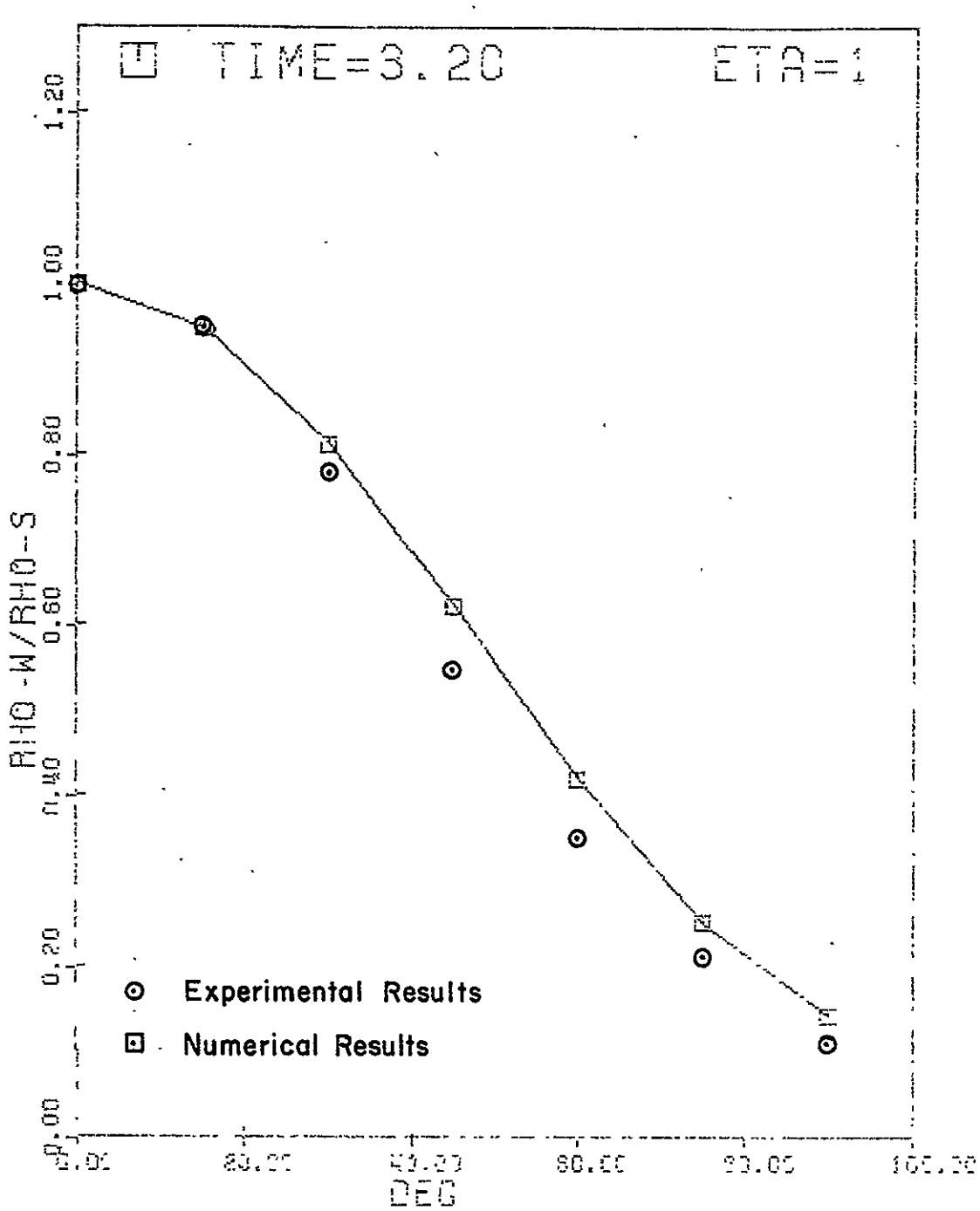


Figure 15. Comparison of Density Distribution with Experimental Results.

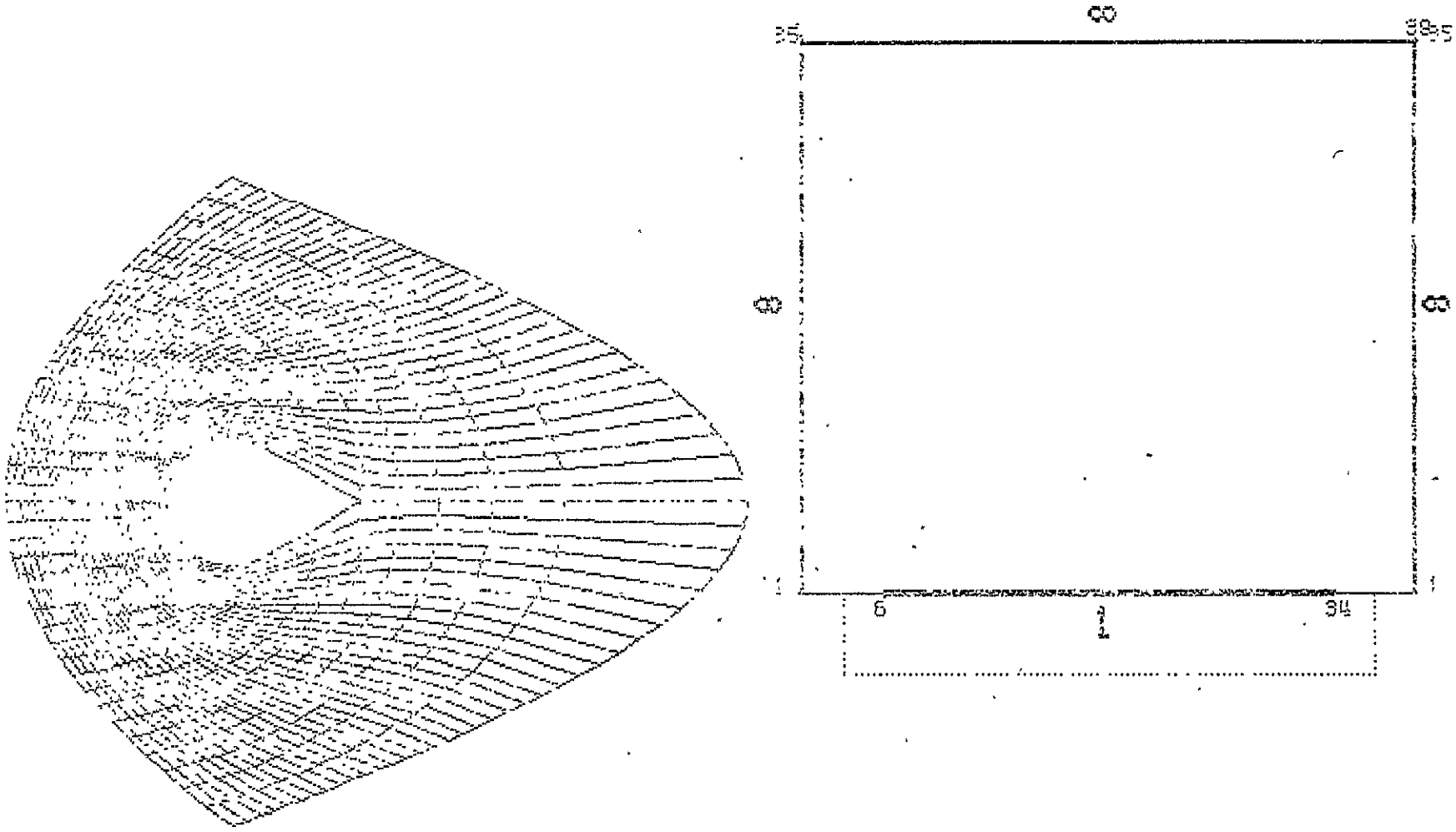


Figure 16. Computational Domain for a Cylinder with an Aft Body.

REPRODUCIBILITY OF THE
ORIGINAL PAGE IS POOR

REPRODUCIBILITY OF THE
ORIGINAL PAGE IS POOR

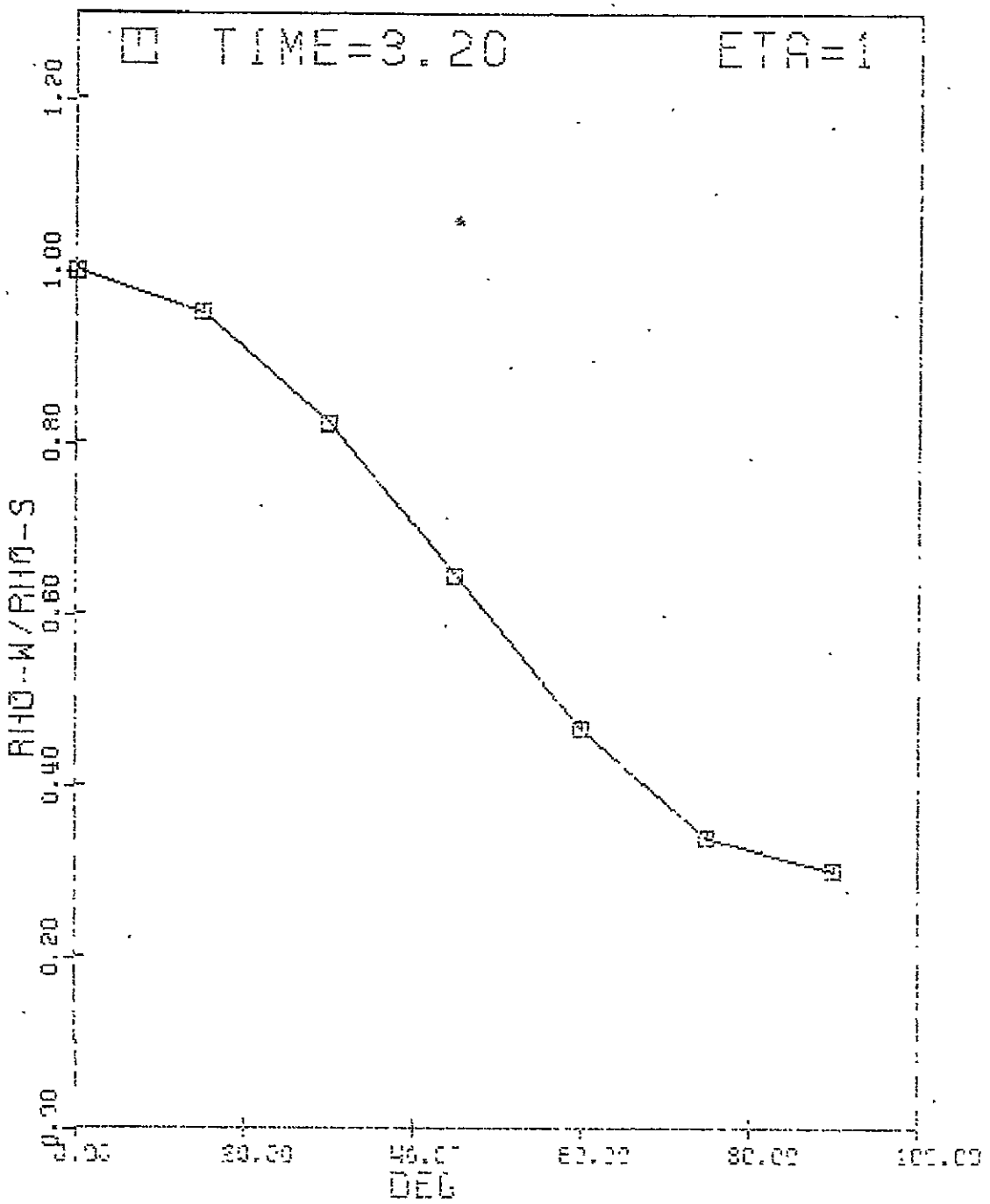

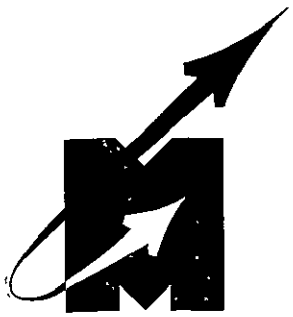
Figure 17. Density Distribution on Cylinder from 0 to 90° for Cylinder with an Aft Body.